Substituent effects on aromatic stacking interactions†

Scott L. Cockroft,[a] Julie Perkins,[a] Cristiano Zonta,[a] Harry Adams,[a] Sharon E. Spey,[a] Caroline M. R. Low,[b] Jeremy G. Vinter,[b] Kevin R. Lawson,[c] Christopher J. Urch[c] and Christopher A. Hunter*[a]

Synthetic supramolecular zipper complexes have been used to quantify substituent effects on the free energies of aromatic stacking interactions. The conformational properties of the complexes have been characterised using NMR spectroscopy in CDCl₃, and by comparison with the solid state structures of model compounds. The structural similarity of the complexes makes it possible to apply the double mutant cycle method to evaluate the magnitudes of 24 different aromatic stacking interactions. The major trends in the interaction energy can be rationalised using a simple model based on electrostatic interactions between the π-faces of the two aromatic rings. However, electrostatic interactions between the substituents of one ring and the π-face of the other make an additional contribution, due to the slight offset in the stacking geometry. This property makes aromatic stacking interactions particularly sensitive to changes in orientation as well as the nature and location of substituents.

Introduction

For decades, researchers from across the chemical sciences have used 'aromatic interactions' to rationalise their observations.[1] Aromatic interactions have been exploited in template-directed synthesis to prepare topologically complex molecules and to control the enantioselectivity of reactions in asymmetric syntheses.[2–5] The arrangements of molecules in solids, liquid crystals and solution are known to be influenced by aromatic stacking interactions.[6–8] In biological systems, aromatic stacking interactions have been identified as key factors in determining the structural and molecular recognition properties of nucleic acids, peptides and proteins.[9–11] For example, X-ray crystal structures have identified stacked aromatic contacts between drug molecules and the aromatic side-chains of proteins.[12–14] These observations have motivated interest in the prediction of stacking interaction energies for use in quantitative structure activity relationships.[15] Whilst *ab initio* calculations[16–22] and qualitative models[23] that describe aromatic stacking interactions exist, experimental data are required to test these theories. Aromatic interactions have been investigated in a range of model systems, which have been extensively reviewed,[24–27] and new studies continue to emerge.

One approach involves the study of *intra*molecular aromatic stacking interactions using rotameric or conformationally flexible molecules.[28–37] Other studies have taken a supramolecular host–guest approach to the assessment of *inter*molecular aromatic interactions.[1,38–40] In the work presented here, we exploit a conformationally well-defined system to measure intermolecular interactions, using hydrogen bonding to force two aromatic rings into a stacked geometry.

The double-mutant cycle is a robust thermodynamic tool that has been employed by numerous researchers to isolate individual weak non-covalent interactions from a noisy background of multiple secondary interactions.[41,42] We have previously used supramolecular zipper complexes in conjunction with the double-mutant cycle approach to quantify a wide range of aromatic interactions, including the effects of substituents on edge-to-face aromatic interactions and cation–π interactions.[43–53] The method was successfully adapted to quantify a number of aromatic stacking interactions (see Fig. 1).[54,55] Since those studies our compound library has been significantly expanded. Here we present a thorough conformational analysis of the complexes and a complete analysis of the entire data set. In the light of the work presented here and the studies of other investigators, we
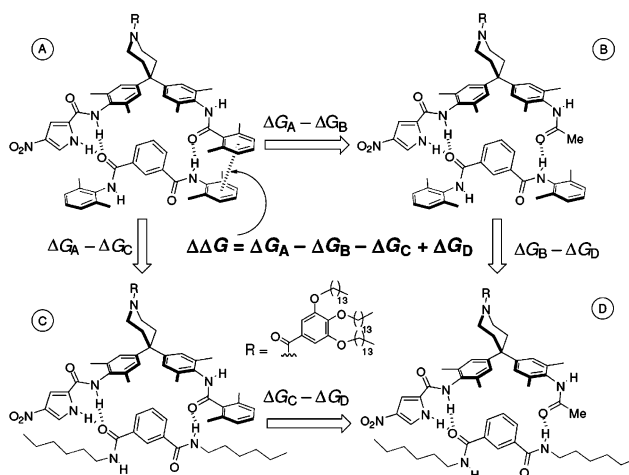

Fig. 1 A chemical double-mutant cycle for measuring the free energy contribution of the aromatic stacking interaction in complex A.

[a]Centre for Chemical Biology, Department of Chemistry, Krebs Institute for Biomolecular Science, University of Sheffield, Sheffield, UK S3 7HF. E-mail: c.hunter@sheffield.ac.uk; Fax: (+44)114 2738673; Tel: (+44)114 2229476

[b]James Black Foundation, 68 Half Moon Road, London, UK SE24 9JE

[c]Syngenta, Jealott's Hill International Research Centre, Bracknell, Berkshire, UK RG42 6EY

† Electronic supplementary information (ESI) available: detailed synthetic procedures and characterisation data for new compounds; crystallographic data (CCDC reference numbers 238547 and 615388–615406). See DOI: 10.1039/b617576g

draw new conclusions concerning the main factors influencing the magnitudes of aromatic stacking interactions.

Design and synthesis

Fig. 1 shows an example of a double-mutant cycle used in this study. The stacking interaction highlighted in complex A is measured by chemical mutations that remove it. A single mutation (*e.g.* comparing the stabilities of complexes A and B) is not sufficient, because this has secondary effects, such as changing the H-bond strength. The double-mutant complex D quantifies these secondary interactions, and the free energy difference of any two parallel mutations in Fig. 1 allows the interaction of interest to be dissected out of the complicated array of weak interactions present in complex A.

The compounds used in this work were prepared as outlined in Fig. 2 and 3. Isophthaloyl derivatives **8a–e**, **9** and **10** were synthesised from the appropriate substituted anilines, which are available commercially or *via* relatively simple syntheses (Fig. 2; ESI†). Bisaniline derivatives **15a–c**, **15e–g** and **20d–f** were prepared according to the routes shown in Fig. 3.

^{1}H NMR titrations were used to measure association constants for 34 different combinations of the isophthaloyl and bisaniline compound libraries. The structural properties of the complexes have been analysed using ^{1}H NMR complexation-induced changes in chemical shifts, ROESY experiments and X-ray crystallography‡ on model compounds. These conformational insights have been used to establish which of the many possible double-mutant cycles can be reliably used to systematically survey the effects of substituents on aromatic stacking interactions.

Solid state conformational studies

Isophthaloyl derivatives **8d**, **8e**, **9** and bisaniline derivatives similar to those used in the ^{1}H NMR titrations of the present study have been successfully crystallised. The conformational attributes of the bisaniline derivatives in the solid state have been discussed previously.[54] The crystal structures of the individual components of a complex are of limited utility, since they provide little information regarding the geometry of the aromatic interactions present in the supramolecular zipper complexes. However, the X-ray crystal structures of simple model compounds have been able to provide a useful indicator of the likely geometry of the edge-to-face aromatic interactions in zipper complexes in solution (Fig. 4a).[43,46,49] The X-ray crystal structures of the model compounds for the edge-to-face zipper complexes reveal H-bonded chains with the head-to-tail packing arrangement shown in Fig. 4a. Based on the
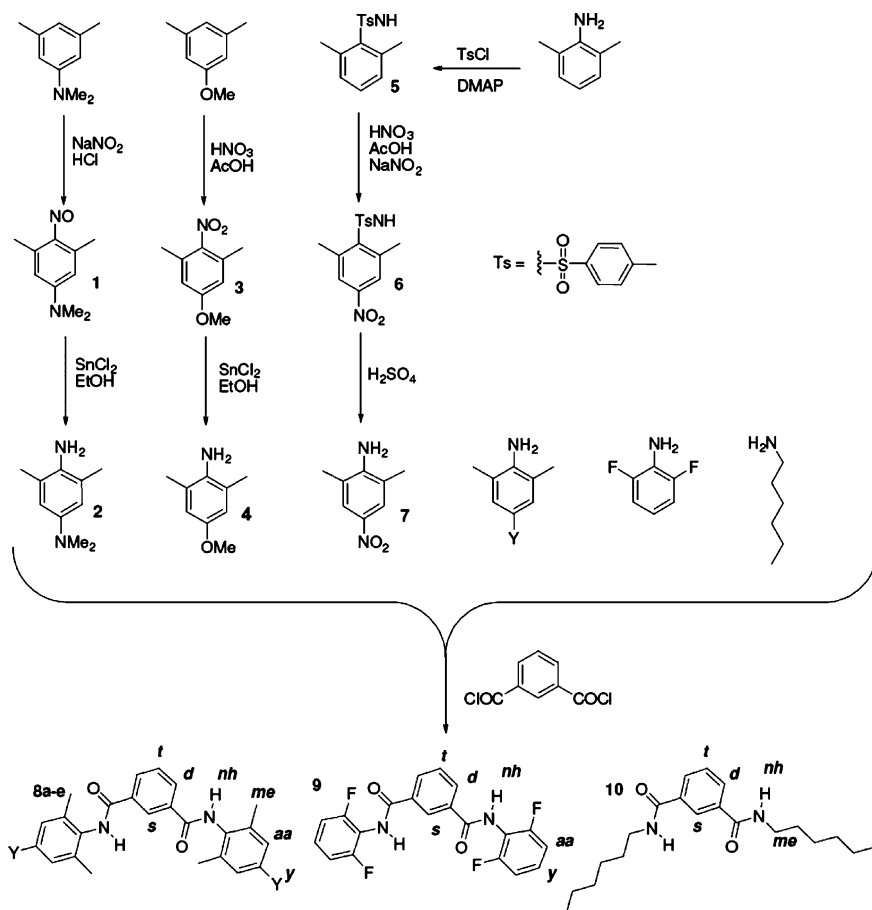
Fig. 2 Synthesis and proton labelling scheme for isophthaloyl derivatives **8a** (Y = NMe₂), **8b** (Y = H), **8c** (Y = OMe), **8d** (Y = Cl), **8e** (Y = NO₂), **9** and **10**.
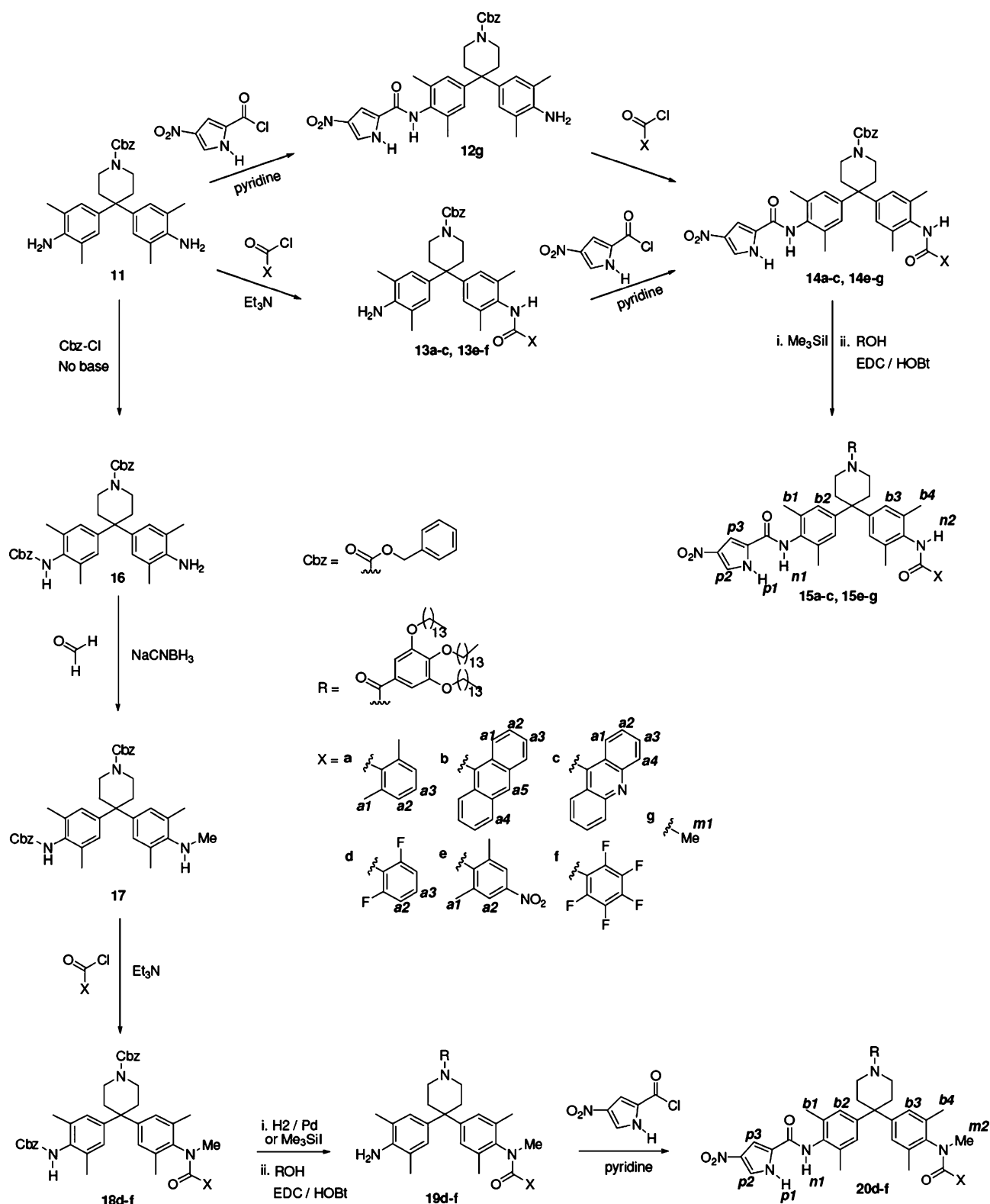
Fig. 3 Synthesis and proton labelling scheme for the **15x** and **20x** series of bisaniline derivatives.

success of this approach, new model compounds were synthesised and crystallised (Fig. 4b and 5). Compounds **21a–24f** held the promise of revealing the geometry of the aromatic stacking interactions in the 'full-sized' zipper complexes (the structures of

compounds **21a**, **21b** and **23d** have been previously deposited in the CCDC).[54,56,57]

Each of the model compounds **21a–24f** were found to form H-bonded chains in the solid state, as expected. However, none of
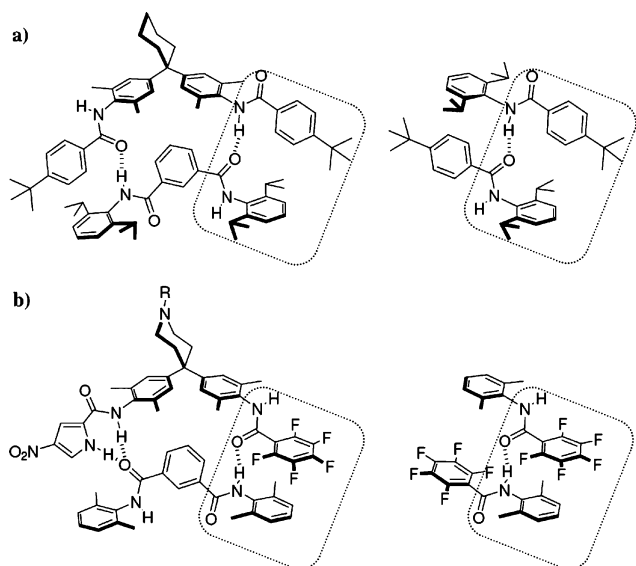
Fig. 4 a) Solid state structures of simple model compounds (right) have previously been used to infer the geometry of edge-to-face aromatic interactions in zipper complexes in solution (left). b) Complex proposed for the measurement of aromatic stacking interactions in solution (left) and the corresponding model compound for X-ray crystallisation studies (right).
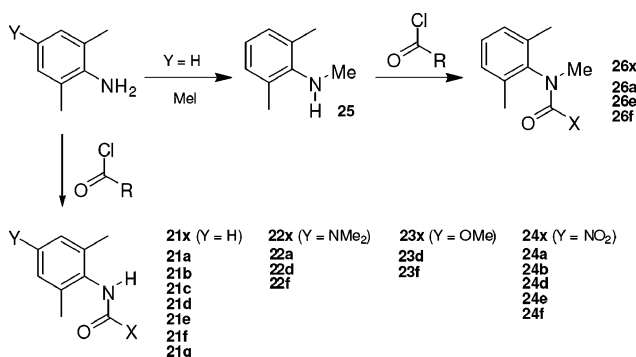

Fig. 5 Model compounds designed to probe the geometry of aromatic stacking interactions in the solid-state. X group labels are shown in Fig. 3.

these compounds crystallised in the desired head-to-tail conformation seen for the edge-to-face model compounds (Fig. 4a). Instead, the stacking compounds crystallised in head-to-head or twisted H-bonded chains. Both of these packing modes were present in the structures of compound **21f**, which was crystallised in two

polymorphic forms (Fig. 6). Based on the propensity of pentafluorophenyl groups to form stacks with electron-rich aromatic systems in the solid state,[6,58–61] it was anticipated that compound **21f** would crystallise in H-bonded chains with head-to-tail stacks in line with the intended design. However, the molecules in the α-polymorph were found to form twisted H-bonded chains accommodating close phenyl–pentafluorophenyl stacking interactions between *adjacent* H-bonded chains (Fig. 6a). In contrast, the β-polymorph forms a parallel head-to-head arrangement containing offset phenyl-phenyl, and pentafluorophenyl–pentafluorophenyl stacks within the H-bonded chain (Fig. 6b).

Whilst the design of the model compounds containing edge-to-face aromatic interactions was successful, the new stacking analogues **21a**–**24f** fall short of the mark. Fig. 4b shows that formation of a stacking interaction on one side of the H-bonded amide chain would create a cavity between the aromatic rings on the opposite side of the dimer. The model compounds shown in Fig. 4a do not suffer from this problem, because edge-to-face aromatic contacts occur on both sides of the H-bonded amide chain, with the 2,6-isopropylated aniline rings providing an additional conformational constraint.[46] In contrast, the aromatic groups in stacking compounds **21a**–**24f** are free to rotate about the H-bonded amide chain. Head-to-head and twisted amide H-bonded chains form in preference to the intended head-to-tail orientation because of the free energy penalty associated with the loss of dispersion interactions in a poorly packed, cavity-filled crystal.

The range of structures obtained for compounds **21a**–**24f**, and the identification of polymorphic forms of **21f** are evidence that there is not a single well-defined pathway involved in the crystallisation of this series of compounds. Nevertheless, useful conformational information can be gained from the X-ray crystal structures of these molecules. Fig. 7 shows that anthracene, acridine, 2,6-dimethylphenyl, or 2,6-fluorophenyl aromatic groups provide sufficient steric influence to twist the aromatic rings out of the plane of the amide bond, which is an essential feature of the supramolecular designs used in this investigation. The aniline rings in compounds **21a**–**24f** are tilted out of the plane of the amide bond by $70° \pm 10°$ (Fig. 7d), and the aromatic rings on the other side of the amide are oriented at $65° \pm 15°$ to the plane of the amide (Fig. 7b). Furthermore, the presence of intermolecular aromatic stacks in the crystal structures demonstrate that close stacking of the terminal aromatic rings in the supramolecular complexes is not sterically compromised by the 2,6-dimethyl and fluorine aromatic substituents.
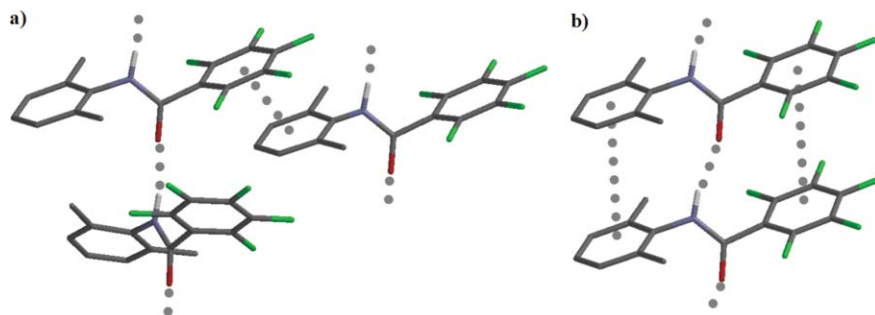

Fig. 6 Interaction motifs in the twisted α-polymorph a) and head-to-head β-polymorph b) of **21f**.
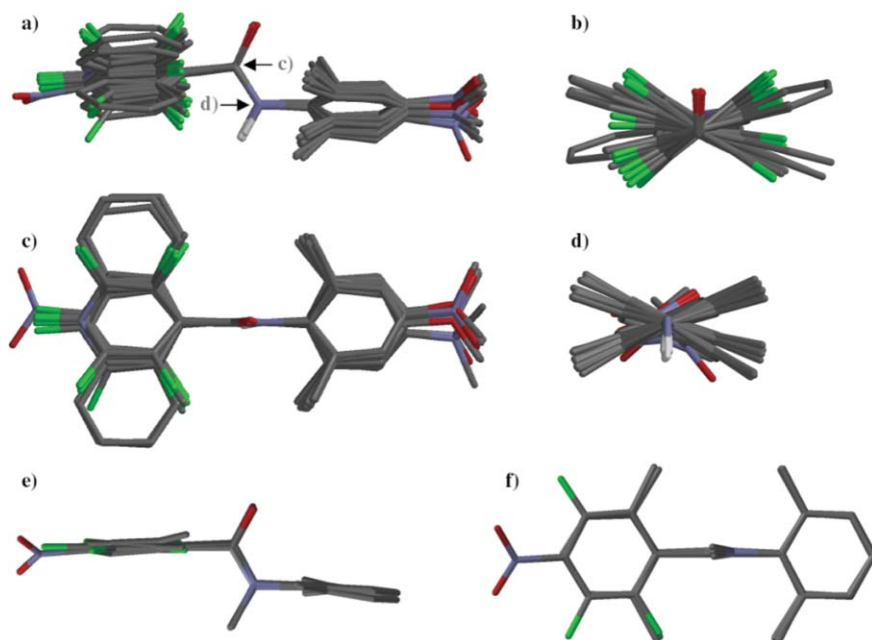
Fig. 7 Overlays of the structures of model compounds in the solid state. a) View of model compounds **21a**–**24f** orthogonal to the amide group. b) View of model compounds **21a**–**24f** along the axis indicated in a). c) View of model compounds **21a**–**24f** in the plane of the amide bond. d) View of model compounds **21a**–**24f** along the axis indicated in a). e) View of *N*-methylamide model compounds **26a**, **26e** and **26f** orthogonal to the amide group. f) View of *N*-methylamide model compounds **26a**, **26e** and **26f** in the plane of the amide bond.

Self-association studies of the isophthaloyl derivatives 8a–10

The solubilities of the isophthaloyl derivatives (Fig. 2) in CDCl$_3$ are in the range 0.2–4 mM. Attempts to determine accurate self-association constants of the isophthaloyl derivatives using ^{1}H NMR dilution experiments were hampered by small observed changes in chemical shift and the limited solubility of these compounds. The dimerisation constants are less than 5 M^{-1}, and since the isophthaloyl derivatives were used as the host at mM concentrations in the ^{1}H NMR titrations, this has a negligible effect on the binding experiments.[48]

Self-association studies of the 15*x* and 20*x* bisaniline derivatives

The nitropyrrole moiety in the bisaniline derivatives (Fig. 3 and 8) is known to promote self-association of these compounds in CDCl$_3$.[54] ^{1}H NMR dilution experiments were performed for each of the bisaniline derivatives, and the data were fit to a dimerisation model. The limiting dimerisation-induced changes in chemical shift and dimerisation constants for each of the bisaniline derivatives are given in Table 1. The large downfield shifts on the nitropyrrole NH (*p1*) and the adjacent amide NH (*n1*) suggest that both of these protons are acting as H-bond donors (Fig. 8c). Each of the bisaniline derivatives also have minor conformers, as seen before in the ^{1}H NMR spectra of **15b**, **15f** and **15g** in CDCl$_3$.[54] The minor conformer (10%) is in slow exchange with the major conformer on the NMR timescale. The minor conformer differs in the chemical shifts of *p1* and *p3*: 9.3 and 5.4 ppm respectively, compared to 9.6 and 7.3 ppm in the major conformer. These differences in chemical shift are consistent with the *cis*-amide shown in Fig. 8b. Although it has previously been shown that
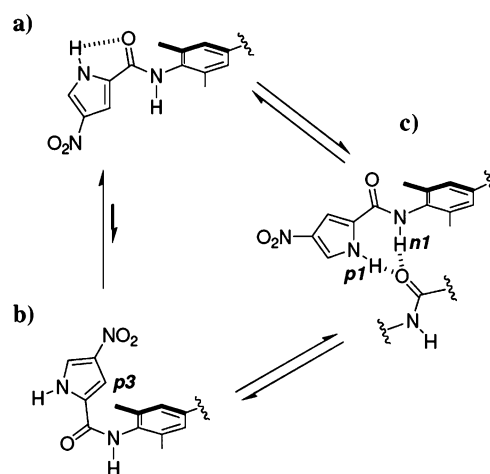

Fig. 8 Conformations of nitropyrrole amides. a) The major conformer of the nitropyrrole moiety in the unbound state. b) ^{1}H NMR experiments indicate a 10% population of the *cis*-amide is in slow exchange with a). The geometry of the *cis*-conformer explains the large upfield change in chemical shift of *p3*. c) In the bound state, the pyrrole NH (*p1*) and the adjacent amide NH (*n1*) signals experience large downfield shifts consistent with the formation of two hydrogen bonds.

the free energy effects of dimerisation cancel in the double-mutant cycle,[54] it is important to account for the effects of dimerisation to obtain accurate $\Delta\delta$ values for the bisaniline guest from ^{1}H NMR titration data (see Experimental section).

Binding studies using the 15*x* bisaniline derivatives

The **15***x* series of bisaniline derivatives were titrated into the isophthaloyl derivatives **8a**, **8b**, **8c**, **8e** and **10**. ^{1}H NMR titration data

1066 | *Org. Biomol. Chem.*, 2007, **5**, 1062–1080

This journal is © The Royal Society of Chemistry 2007

Table 1 Dimerisation constants K_{dim} (M^{-1}) and limiting dimerisation-induced changes in ^1H chemical shift (ppm) for the bisaniline derivative series **15x** and **30x** in $CDCl_3$ at 298 K[a]

| | Signal | | | | | | | | | | | | | |
Compound	K_{dim}	p1	p2	n1	n2	b1	b2	b3	b4	a1	a2	a3	a4	a5	m1/m2
15a	9 ± 2	2.4	−0.7	2.3	0.7	−0.3	−0.2	0.0	−0.1	−0.3	−0.3	−0.2	—	—	—
15b	13 ± 2	2.2	−0.8	2.0	0.6	−0.4	−0.3	−0.1	−0.2	−0.3	−0.3	−0.3	−0.2	−0.3	—
15c	14 ± 2	2.5	−0.7	2.1	1.9	−0.3	−0.2	−0.1	−0.1	−0.6	−0.5	−0.4	−0.4	—	—
15f	11 ± 2	2.2	−0.5	2.7	1.2	−0.2	−0.1	−0.1	−0.1	—	—	—	—	—	—
15g	20 ± 2	2.5	−0.7	2.0	1.1	−0.3	−0.2	−0.1	−0.2	−0.2	—	—	—	—	−0.2
20d	33 ± 5	2.3	−0.7	2.2	—	−0.3	−0.2	0.0	−0.1	—	−0.2	−0.2	—	—	−0.1
20e	30 ± 4	2.6	−0.7	2.5	—	−0.5	−0.3	−0.1	−0.1	−0.3	−0.2	—	—	—	−0.1
20f	16 ± 6	2.7	−0.6	2.4	—	−0.3	−0.2	−0.2	−0.1	—	—	—	—	—	−0.2

[a] See Fig. 3 for proton labelling scheme. **p3** shifts could not be accurately determined due to overlap with the residual $CHCl_3$ peak throughout most of the ^1H NMR experiments. There were no significant changes in the chemical shift of the signals for protons on the piperidine ring or solubilising group. Dilution experiments were repeated at least twice, and K_{dim} is the weighted mean based on the observed changes in chemical shift for all signals monitored. The error is twice the standard error.

were fit to a 1 : 1 binding isotherm that allowed for dimerisation of the guest. The bisaniline derivatives contain a large solubilising group, intended to facilitate their use as guest molecules in ^1H NMR titrations. Despite the solubilising group, the nitro derivative **15e** was poorly soluble in $CDCl_3$ (~3 mM). Analysis of host ^1H NMR chemical shifts from titration experiments with **15e** gave less than 15% coverage of the binding isotherm, preventing the simultaneous determination of reliable 1 : 1 host–guest association constants and $\Delta\delta$ values. Accordingly, further studies with **15e** were abandoned. The pentafluorophenyl compound **15f** also suffered from low solubility in $CDCl_3$ (~10 mM); in the worst case 30% of compound **10** was bound at the end of the **10** : **15f** titration, although the favourable binding of **8a** with **15f** allowed 70% coverage of the **8a** : **15f** binding isotherm. All of the other compounds in the **15x** series had sufficient solubility in $CDCl_3$ (~35–40 mM) to allow the accurate determination of association constants and $\Delta\delta$ values.

ROESY studies of complexation

Valid application of the double-mutant cycle methodology requires that the core structure of each complex is conserved. It is therefore important to check the geometries of the complexes before attempting to determine (and interpret) interaction free energies. Intermolecular NOEs from two-dimensional ROESY experiments provide limited, but useful information about the structures of the complexes (Table 2 and Fig. 9). The NOEs **b1–d** and **b4–d** are consistently observed indicating that the isophthaloyl group is docked into the bisaniline pocket in the core of the complex. Other NOEs confirm that the nitropyrrole group sits over the terminal aromatic ring in at least three of the complexes (**p2–me**), and that on the opposite side of the complex the anthracene group in bisaniline derivative **15b** is in close proximity to the terminal aniline rings of the isophthaloyl derivatives (**a1–me** and **a2–me**).

Table 2 Intermolecular NOEs observed in two-dimensional ROESY experiments[a]

| | Bisaniline compound | | | | |
Isophthaloyl compound	**15a** X = o-Me$_2$-phenyl	**15b** X = anthracene	**15c** X = acridine	**15f** X = F$_5$-phenyl	**15g** X = Me
8a Y = NMe$_2$	b4–d	b1–d p2–me a1–me a2–me	b1–d b4–d	b1–d b4–d	b4–d
8b Y = H	b1–d b4–d	b1–d [b] b4–d p2–me a1–me a2–me	b1–d b4–d	b1–d[b] b4–d	b1–d [b]
8c Y = OMe	b1–d b4–d p2–me	n.d.[c]	n.d.	b1–d b4–d	n.d.
10	b1–d b4–d	b1–d[b] b4–d a1–nh	b4–d	b1–d [b] b4–d	b1–d[b] b4–d

[a] See Fig. 2 and 3 for proton labelling schemes. Experiments were carried out on 1 : 1 mixtures of the two components in $CDCl_3$ at the maximum concentration possible 0.2–5 mM. Intermolecular NOEs of complexes with compounds **8d**, **8e** and **9** were not detectable because of their low solubilities in $CDCl_3$. [b] Previously reported but included for comparison purposes. [c] Not determined.
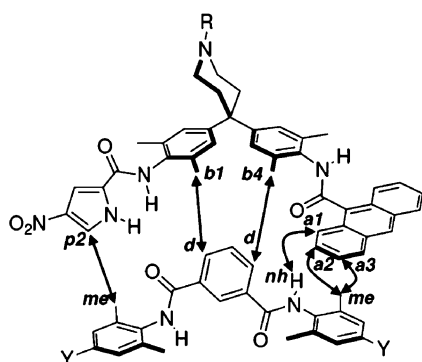
Fig. 9 Intermolecular NOEs observed for the complexes of the **15x** series of bisaniline derivatives with compounds **8a–c** and **10**.

Complexation-induced changes in chemical shift of the isophthaloyl hosts 8x, 9 and 10

Complexation-induced changes in chemical shift ($\Delta\delta$) can be determined from ^{1}H NMR titrations and are a particularly rich source of structural information. $\Delta\delta$ Values for the hosts are easily obtained from the direct extrapolation of ^{1}H NMR binding curves to the 100% bound state. Table 3 lists the $\Delta\delta$ values for all of the isophthaloyl hosts **8a–8e**, **9** and **10** in each titration experiment. There are consistent patterns in the changes in chemical shift. The large upfield shifts of the *d* and *t* signals indicate that these protons are docked into the bisaniline aromatic cleft. The large downfield shifts on the amide *nh* show that it is involved in hydrogen bonding. The signals on the terminal aromatic rings (*me*, *aa*) experience moderate upfield shift changes that are consistent with the shielding effect of the aromatic stack that is formed upon complexation. The magnitude of these changes is generally larger in the anthracene (**15b**) and acridine (**15c**) complexes, where there are extended aromatic surfaces with larger ring currents, and lower in the single mutant (**15g**) complexes, where the aromatic group is replaced by a methyl group.

Not all of the complexes are so well behaved. Attention is immediately drawn to the *s* signal of the **8b·15c** complex that experiences a surprisingly large upfield shift. In addition to this unusual chemical shift behaviour, the titration data did not fit well to a 1 : 1 complexation model but was well described by a 2 : 1 (guest–host) model which included dimerisation of the bisaniline guest. Molecular modelling using XED[62] provided a plausible explanation for this anomalous behaviour. The 1 : 1 **8b·15c** complex is the ideal geometry to bind a second **15c** molecule. The structure of the XED-minimised 2 : 1 complex is shown in Fig. 10 and accounts for the strange patterns of chemical shifts that we observe for this complex. The acridine nitrogen of the first **15c** molecule is capable of accepting two H-bonds from the nitropyrrole group of the second **15c** molecule. The *s* proton is held directly over the acridine ring of the second **15c** molecule, and this is the reason for the large upfield shift of *s*. Similarly, the *aa* and *y* protons form a favourable edge–face interaction with one of the **15c** aniline rings, explaining their large upfield complexation-induced changes in chemical shift. The other signals are unaffected relative to the other complexes, since their environment is not altered by formation of the 2 : 1 complex. The final piece of support for the assembly presented in Fig. 10 comes from the binding properties of **15c** with the other isophthaloyl derivatives. Both **8a** (Y = NMe$_2$) and **8e** (Y = NO$_2$) bind to **15c** following a 1 : 1 binding isotherm (rather than 2 : 1), with very similar $\Delta\delta$ values to those obtained with the anthracene bisaniline derivative **15b**. This is because the *p*-nitro and *p*-dimethylamino Y-substituents of compounds **8a** and **8e** are too large to be accommodated in the same the position as the *y* proton in the bisaniline pocket of the second **15c** molecule in the 2 : 1 complex.

The *s* proton in the isophthaloyl hexyl mutant **10·15c** complex also experiences an upfield complexation-induced change in chemical shift. This indicates that the complex may be similar to the **8b·15c** complex discussed above. Accordingly, the acridine complexes will not be used to construct double-mutant cycles.
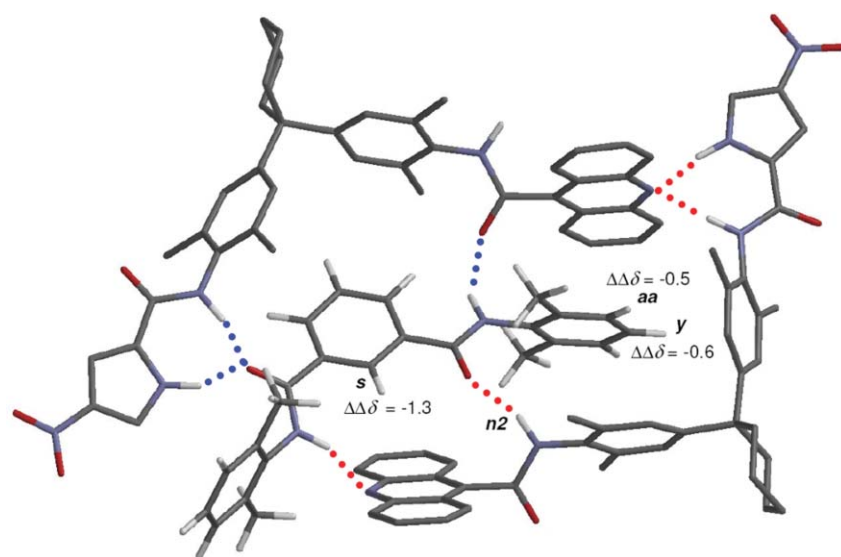

Fig. 10 Energy minimised structure showing how the **8b·15c** complex (blue H-bonds) is able to bind a second molecule of **15c** (red H-bonds). This structure is consistent with the unusual complexation-induced chemical shift changes of the labelled protons. The $\Delta\Delta\delta$ values are the additional changes in chemical shift for this complex compared to the simple 1 : 1 complexes. The solubilising group and non-polar protons of **15c** are omitted for clarity.

Table 3 Limiting complexation-induced changes in ^{1}H chemical shift ($\Delta\delta$ in ppm) from NMR titrations in CDCl$_3$ at 298 K for isophthaloyl host series **8a–e**, **9** and **10**

| Guest | Aromatic group | Host | Y | Signal | | | | | | |
				d	t	nh	aa	me	s	y
Complex A										
15a	o-Me$_2$-phenyl	**8a**	NMe$_2$	−0.34	−1.07	1.46	−0.14	−0.20	0.21	−0.02
15b	anthracene	**8a**	NMe$_2$	−0.32	−1.08	1.55	−0.37	−0.38	0.16	−0.06
15c	acridine	**8a**	NMe$_2$	−0.41	−1.09	1.54	−0.47	−0.46	0.02	−0.11
15f	F$_5$-phenyl	**8a**	NMe$_2$	−0.51	−1.23	1.10	−0.12	−0.19	0.03	0.01
20d	o-F$_2$-phenyl	**8a**	NMe$_2$	−0.49	−1.35	1.59	−0.17	−0.23	0.16	−0.02
20e	p-NO$_2$-o-Me$_2$-phenyl	**8a**	NMe$_2$	−0.49	−1.48	1.66	−0.23	−0.24	0.15	−0.02
20f	F$_5$-phenyl	**8a**	NMe$_2$	−0.57	−1.47	1.62	−0.14	−0.20	0.13	0.03
15a	o-Me$_2$-phenyl	**8b**	H	−0.29	−0.97	1.58	−0.19	−0.25	0.25	so^b
15b	anthracene	**8b**	H	−0.34	−1.04	1.70	−0.40	−0.42	0.24	−0.19
15c	acridine	**8b**	H	−0.73^c	−1.16^c	2.09^c	−0.73^c	−0.42^c	−1.12^c	−0.75^c
15f	F$_5$-phenyl	**8b**	H	−0.48	−1.20	1.31	−0.15	−0.24	0.10	−0.08
20d	o-F$_2$-phenyl	**8b**	H	−0.44	−1.22	1.78	−0.19	−0.25	0.23	−0.12
20e	p-NO$_2$-o-Me$_2$-phenyl	**8b**	H	−0.45	−1.32	1.82	−0.21	−0.27	0.17	−0.10
20f	F$_5$-phenyl	**8b**	H	−0.52	−1.34	1.74	−0.12	−0.22	0.19	−0.04
15a	o-Me$_2$-phenyl	**8c**	OMe	−0.30	−0.96	1.48	−0.18	−0.25	0.21	−0.04
15f	F$_5$-phenyl	**8c**	OMe	−0.51	−1.14	1.51	−0.14	−0.20	0.07	−0.01
20d	o-F$_2$-phenyl	**8c**	OMe	−0.46	−1.33	1.67	−0.20	−0.26	0.20	−0.02
20f	F$_5$-phenyl	**8c**	OMe	−0.53	−1.39	1.76	−0.14	−0.24	0.18	0.01
15a	o-Me$_2$-phenyl	**8d**	Cl	−0.24	−0.82	1.66	−0.39	−0.29	0.25	—
20d	o-F$_2$-phenyl	**8d**	Cl	−0.38	−1.14	1.81	−0.29	−0.26	0.20	—
20f	F$_5$-phenyl	**8d**	Cl	−0.38	−1.09	1.81	−0.32	−0.30	0.23	—
15a	o-Me$_2$-phenyl	**8e**	NO$_2$	−0.06	−0.49	1.70	−0.34	−0.26	0.44	—
15b	anthracene	**8e**	NO$_2$	−0.27	−0.83	1.67	−0.61	−0.46	0.20	—
15c	acridine	**8e**	NO$_2$	−0.18	−0.83	1.61	−0.42	−0.34	0.17	—
15f	F$_5$-phenyl	**8e**	NO$_2$	−0.05	−0.30	1.31	−0.30	−0.24	0.41	—
20d	o-F$_2$-phenyl	**8e**	NO$_2$	−0.28	so	1.80	−0.32	−0.29	0.26	—
20d	p-NO$_2$-o-Me$_2$-phenyl	**8e**	NO$_2$	−0.19	−0.62	1.76	−0.31	−0.26	0.40	—
20f	F$_5$-phenyl	**8e**	NO$_2$	−0.19	−0.59	1.68	−0.34	−0.30	0.40	—
15a	o-Me$_2$-phenyl	**9**	—	−0.33	−0.74	1.76	−0.22	—	0.23	so
20d	o-F$_2$-phenyl	**9**	—	−0.31	−0.74	2.09	so	—	0.24	so
20f	F$_5$-phenyl	**9**	—	−0.36	−0.82	1.87	−0.21	—	0.24	so
Complex B										
15g	—	**8a**	NMe$_2$	−0.48	−1.23	1.34	−0.06	−0.12	0.14	0.00
15g	—	**8b**	H	−0.43	−1.12	1.65	−0.15	−0.18	0.23	−0.09
15g	—	**8c**	OMe	−0.43	−1.02	1.45	−0.12	−0.18	0.18	−0.06
15g	—	**8d**	Cl	−0.33	−0.92	1.88	−0.36	−0.31	0.29	—
15g	—	**8e**	NO$_2$	−0.15	−0.53	1.86	−0.33	−0.25	0.53	—
15g	—	**9**	—	−0.44	−0.89	1.95	so	—	0.23	so
Complex C										
15a	o-Me$_2$-phenyl	**10**	—	−0.38	−1.00	1.07	—	−0.28	0.08	—
15b	anthracene	**10**	—	−0.42	−1.11	1.02	—	−0.41	0.03	—
15c	acridine	**10**	—	−0.63	−1.06	0.89	—	−0.55	−0.24	—
15f	F$_5$-phenyl	**10**	—	−0.49	−0.69	0.58	—	−0.27	0.02	—
20d	o-F$_2$-phenyl	**10**	—	−0.45	−1.00	1.21	—	−0.26	0.05	—
20e	p-NO$_2$-o-Me$_2$-phenyl	**10**	—	−0.41	−1.02	1.22	—	−0.27	0.11	—
20f	F$_5$-phenyl	**10**	—	−0.45	−0.91	1.22	—	−0.32	0.09	—
Complex D										
15g	—	**10**	—	−0.43	−0.89	1.01	—	−0.21	0.06	—

^{a} See Fig. 2 for proton labelling scheme. Titrations were performed at least twice. ^{b} so—Not determined due to signal overlap. ^{c} Data for the **8b·15c** complex were fit to a 2:1 model (guest:host) including dimerisation of the guest.

Complexation-induced changes in chemical shift of the 15x bisaniline guests

The qualitative interpretations of host $\Delta\delta$ values presented above can provide a lot of information about the structure of a complex, but this is only half the story, as the complexation-induced changes in chemical shift of the bisaniline guests have yet to be discussed. $\Delta\delta$ Values for the guest molecules can be determined by separating the contributions of guest dimerisation and host–guest complexation to the observed chemical shifts changes (see Experimental section). The $\Delta\delta$ values for all of the bisaniline guests in the complexes with isophthaloyl derivatives **8a**, **8b**, **8c** and **10**, are given in Table 4. The intermolecular hydrogen bonds in the zipper complexes are a crucial part of the supramolecular design. They have a central role in stabilising and controlling the geometry of the complexes. The bisaniline derivatives in the **15x** series contain three substantial H-bond donors. The $\Delta\delta$ values of these NH protons enable any structural irregularities in the complexes to be easily identified. The nitropyrrole **p1** and **n1** signals should have large positive $\Delta\delta$ values from the formation of H-bonds in the complex

This journal is © The Royal Society of Chemistry 2007

Org. Biomol. Chem., 2007, **5**, 1062–1080 | 1069

and the *n2* signal should have zero (or a small) change in chemical shift, since it should not be involved in H-bonding. This was found to be the case for all of the **15x** complexes, except in two situations. Firstly, the **10·15c** complex, which has already been identified as having conformational problems from the host Δδ values, has a larger than expected shift for *n2*, consistent with the structure of the 2 : 1 complex shown in Fig. 10. The second case affects all complexes containing **15f**. Δδ Values of *n2* in complexes with **15f** range from +0.5 ppm in the complex with **8a**, to +2.2 ppm in the complex with **8c**. Previous observation of this anomalous shift in the **8b·15f** complex was attributed to dimerisation.[54] However, dimerisation cannot be the cause, because it has been taken into account in determination of the guest Δδ values presented in Table 4.

Comparing the Δδ values of the **15f** complexes with the others in Tables 3 and 4 also exposes reduced complexation-induced shifts for the nitropyrrole *p1* and *n1* guest signals. The shifts of the isophthaloyl host signals *nh* and *aa* are also reduced in these complexes, but the *d* and *t* signals remain relatively unaffected. Clearly, the *n2* amide proton adjacent to the pentafluorophenyl group is acting as a H-bond donor in the **15f** complexes. The shift patterns described above can be explained by the equilibria shown in Fig. 11. When Y = NMe₂ (**8a**) the equilibria lie to the left (conformers a and c) as indicated by the smallest *n2* Δδ of the **15f** complexes. In conformers b and d on the right-hand side of the equilibria in Fig. 11, the *nh* amide breaks its H-bond with the carbonyl adjacent to the pentafluorophenyl ring. The *n2* Δδ values signify that the intermolecular stacking interaction that we wish to measure is not present to a significant extent in the **8x·15f** complexes. The physical basis for this conformational problem seems to lie with the electron-withdrawing pentafluorophenyl group in **15f**, which makes the amide adjacent to the pentafluorophenyl ring a poor H-bond acceptor, but a good H-bond donor. This problem should affect all bisaniline derivatives containing electron-withdrawing aromatic rings, but there is a simple solution. New bisaniline derivatives **20d**, **20e** and **20f** were synthesised by the route shown in Fig. 3 to replace the offending amide proton with a methyl group, blocking access to conformers b and d in Fig. 11.

Conformational properties of the 20x *N*-methylamide bisaniline derivatives

The corresponding model compounds for the *N*-methylamide bisaniline derivatives **20e** and **20f** (**26e** and **26f**) were synthesised by the route shown in Fig. 5. The crystal structure of related compound **26a** has been previously determined and is included for comparison in the structural overlays in Fig. 7e and f.[56] In the solid state, the aromatic rings in all three model compounds are twisted 90° out of the plane of the *N*-methylamide; the ideal geometry for the zipper complexes. The steric effects of substituents on the aromatic rings influence the position of the amide *cis–trans* equilibrium.[63] Previous studies have shown that the four methyl groups *ortho* to the amide in compound **26a** ensure that it is found exclusively in the *trans*-conformation in CDCl₃, just as it is in the solid state (Fig. 7e).[56] Similarly, the ¹H NMR spectra of model compound **26e**, the bisaniline precursors **18e** and **19e**, and the final bisaniline guest compound **20e** only showed the presence of the *trans*-amide conformer. In contrast, the ¹H and ¹⁹F NMR

spectra of model compound **26f**, precursors **18d**, **18e**, **19d**, **19e**, and the final bisaniline guest compounds **20d** and **20f** all showed the presence of both *cis*- and *trans*-amide conformers in slow exchange. Integration of the *N*-methyl ¹H NMR signals indicated a 30% population of the unwanted *cis*-conformer in CDCl₃ for all of these fluoroaromatic compounds.

Each of the *N*-methylated bisaniline derivatives **20d**, **20e** and **20f** were very soluble in CDCl₃ compared to the non-methylated equivalents, so it seems that the polar amide NH (*n2*) was a major contributor to low solubility as postulated earlier. The improved solubility of the **20x** series of bisaniline derivatives allowed large fractions of the binding isotherms to be covered (up to 90%) which improved the accuracy of the binding constant and Δδ value determinations. NMR titration data for **20e** were fit to a 1 : 1 model including dimerisation of the guest, as for the **15x** bisaniline derivatives. Limiting dimerisation-induced changes in chemical shift for the **20x** bisaniline derivatives are included in Table 1. The *cis–trans* amide ratio of compounds **20d** and **20f** did not change during the titrations, because the guest molecules were present in large excess during most of the experiment, and the rate of equilibration is on the time-scale of hours. Titration data obtained using compounds **20d** and **20f** were therefore fit to a 1 : 1 model including dimerisation of the guest, with the concentration of guest corrected to account for the proportion of inactive *cis*-conformer (as determined by integration of the *N*-methyl *m2/m2* + signals). The *trans N*-methyl signals *m2* of compounds **20d** and **20f** showed small positive changes in chemical shift, but the *cis N*-methyl *m2+* signals did not change during the titration, confirming that the *cis* isomers do not bind to the isophthaloyl derivatives (Table 4). Δδ Values for the hosts (**8a–e**, **9** and **10**) and the **20x** guests used in the NMR titrations are included in Tables 3 and 4, alongside the values obtained for the **15x** complexes.

NMR solution structure determination of complexes

So far, we have used Δδ values to characterise the structures of the complexes in a qualitative fashion. However, it is possible to use Δδ values in a quantitative manner to gain a clearer view of the conformational ensemble of the zipper complexes. We have developed a computational method for determining the three-dimensional structures of intermolecular complexes in solution using Δδ values. This approach has been shown to give high-resolution structural information that agrees well with the corresponding X-ray crystal structures where they are available.[57,64–67] This method has been used to determine the solution structures of nine representative complexes containing the isophthaloyl derivatives **8a–c**, and bisaniline derivatives **15a**, **15b**, **15g**, **20d**, **20e** and **20f**. The calculated Δδ values of the optimised structures shown in Fig. 12 are in excellent agreement with the experimental values (Table 5). While the absolute magnitudes of the Δδ values vary from one complex to another, the patterns are very similar and the corresponding structures of the complexes are remarkably consistent. The geometry of the stacked region of the complex appears to be particularly well defined and is unaffected by the magnitude of the aromatic stacking interaction (the **8a·15a** complex contains the most repulsive stacking interaction in the zipper complexes, and the **8a·20f** complex the most attractive, see later).

Table 4 Limiting complexation-induced changes in ¹H chemical shift (Δδ in ppm) from NMR titrations in CDCl₃ at 298 K for bisaniline guest series **15x** and **20x**[a]

Guest	Aromatic group	Host	Y	Bisaniline signal												
				p1	p2	n1	m2 n2	b1	b2	b3	b4	m1 a1	a2	a3	a4	m2+ a5
Complex A																
15a	o-Me₂-phenyl	8a	NMe₂	2.3	-1.1	2.1	0.1	-0.1	0.0	0.1	0.0	-0.2	-0.2	-0.1	—	—
15b	anthracene	8a	NMe₂	2.1	-1.0	1.9	0.1	-0.1	0.0	0.1	0.0	-0.2	-0.1	-0.1	-0.1	-0.2
15c	acridine	8a	NMe₂	2.4	-1.2	2.3	0.3	-0.1	0.0	0.2	0.0	-0.2	-0.1	-0.1	-0.2	—
15f	F₅-phenyl	8a	NMe₂	1.1	-0.8	1.4	0.5	0.0	0.1	0.1	0.0	—	—	—	—	—
20d	o-F₂-phenyl	8a	NMe₂	2.5	-0.9	2.6	0.0	-0.1	0.0	0.2	0.0	—	-0.4	-0.2	—	0.0
20e	p-NO₂-o-Me₂-phenyl	8a	NMe₂	2.6	-0.8	2.7	0.1	-0.1	0.1	0.2	0.1	-0.2	-0.4	—	—	—
20f	F₅-phenyl	8a	NMe₂	2.4	-0.6	2.5	0.0	-0.1	0.1	0.2	0.1	—	—	—	—	0.0
15a	o-Me₂-phenyl	8b	H	1.9	-1.1	2.0	0.2	-0.2	0.0	0.1	0.0	-0.3	-0.3	-0.1	—	0.0
15b	anthracene	8b	H	2.5	-1.5	2.5	0.2	-0.2	0.0	0.2	0.0	-0.3	-0.1	-0.1	-0.2	0.0
15c	acridine	8b	H	b	b	b	b	b	b	b	b	b	b	b	b	b
15f	F₅-phenyl	8b	H	0.7	-1.4	1.8	1.4	-0.1	0.1	0.2	0.0	—	-0.3	-0.1	—	0.0
20d	o-F₂-phenyl	8b	H	2.1	-1.3	2.2	0.0	-0.2	0.0	0.2	0.0	-0.2	-0.3	—	—	—
20e	p-NO₂-o-Me₂-phenyl	8b	H	2.0	-1.3	2.4	0.1	-0.1	0.0	0.2	0.0	-0.2	—	—	—	0.0
20f	F₅-phenyl	8b	H	2.3	-1.2	2.7	0.0	-0.1	0.1	0.2	0.1	-0.2	—	-0.1	—	0.0
15a	o-Me₂-phenyl	8c	OMe	1.9	-0.9	1.8	0.2	-0.1	0.0	0.1	0.0	-0.2	-0.2	—	—	—
15f	F₅-phenyl	8c	OMe	1.7	-1.1	2.7	2.2	-0.1	0.1	0.2	-0.1	—	—	—	—	—
20d	o-F₂-phenyl	8c	OMe	2.6	-1.5	2.7	0.0	-0.2	0.0	0.2	0.0	—	-0.4	-0.2	—	0.0
20f	F₅-phenyl	8c	OMe	2.5	-1.4	1.9	0.0	-0.1	0.1	0.2	0.1	—	—	—	—	0.0
Complex B																
15g	—	8a	NMe₂	1.8	-0.9	1.7	0.2	-0.1	0.0	0.1	0.0	-0.2	—	—	—	—
15g	—	8b	H	2.0	-1.3	2.4	0.4	-0.2	0.0	0.2	-0.1	-0.4	—	—	—	—
15g	—	8c	OMe	2.2	-1.1	2.3	0.4	-0.2	0.0	0.3	0.0	-0.3	—	—	—	—
Complex C																
15a	o-Me₂-phenyl	10	—	1.9	-0.2	3.0	0.3	-0.2	0.0	0.1	0.0	0.0	-0.1	0.0	—	0.0
15b	anthracene	10	—	1.9	-0.2	3.2	0.3	-0.2	0.0	0.2	0.0	-0.1	0.0	0.0	0.0	—
15c	acridine	10	—	1.9	-0.1	3.0	0.8	-0.1	0.0	0.1	0.1	-0.1	-0.1	0.0	-0.1	—
15f	F₅-phenyl	10	—	1.2	-0.1	1.7	0.6	-0.1	0.0	0.0	0.0	—	—	—	—	—
20d	o-F₂-phenyl	10	—	2.0	-0.2	2.8	0.0	-0.1	0.0	0.2	0.0	—	0.0	0.0	—	0.0
20e	p-NO₂-o-Me₂-phenyl	10	—	2.2	-0.2	3.4	0.1	-0.2	0.0	0.1	0.0	0.0	0.0	0.0	—	—
20f	F₅-phenyl	10	—	2.6	-0.2	3.2	0.1	-0.2	-0.1	0.1	0.0	—	—	—	—	0.0
Complex D																
15g	—	10	—	2.2	-0.1	2.8	0.5	-0.1	-0.1	0.2	-0.1	-0.2	—	—	—	—

[a] See Fig. 3 for proton labelling scheme. *p3* shifts could not be accurately determined due to significant overlap with the residual CHCl₃ peak throughout most of the ¹H NMR experiments. The low solubilities of **8d**, **8e** and **9** result in <5% bound guest, preventing accurate determination of Δδ values. There were no significant changes in the chemical shift of the signals for protons on the piperidine ring or solubilising group. Titration experiments were repeated at least twice and Δδ is the weighted mean based on the % bound guest at the point from which the Δδ value was extrapolated. [b] Data for the **8b**·**15c** complex were fit to a 2 : 1 model (guest : host) preventing Δδ determination with the methods used.

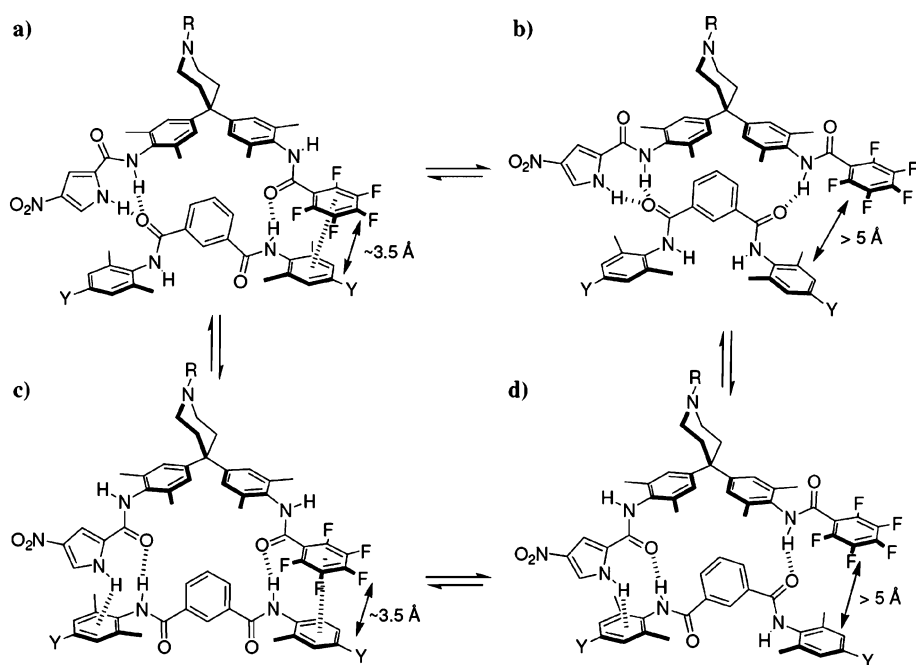**Fig. 11** Conformational equilibria of **15f** complexes. Δδ Values indicate that **15f** is not only able to complex the isophthaloyl hosts in its intended binding mode a), but also in conformations b) and d) where rearrangement of the amide H-bonds disrupts the intermolecular stacking interaction.
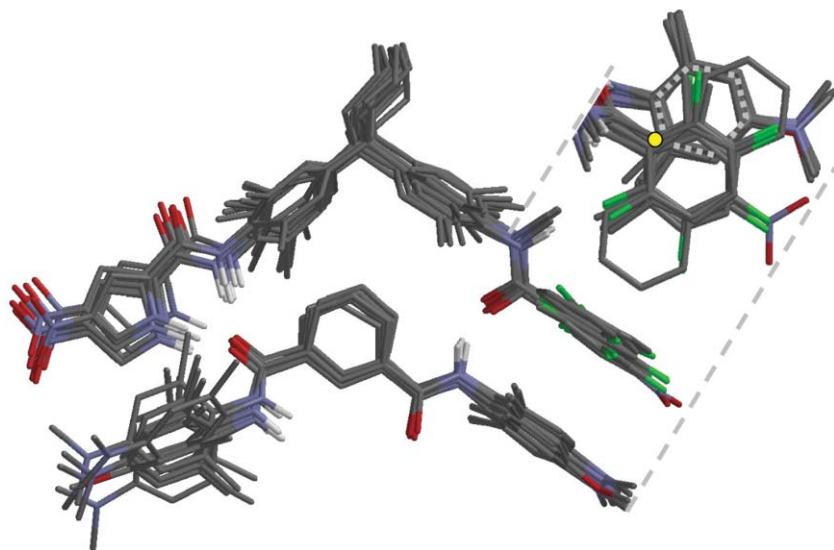

Fig. 12 Overlay of solution structures calculated from the Δδ values in Table 5. The inset shows the geometry of the offset aromatic stacks. The dotted grey ring shows the position of the aniline rings of the isophthaloyl derivatives, and the yellow dot indicates the position of the *m1* methyl carbon in compound **15g**.

The determination of guest Δδ values in complexes containing isophthaloyl derivatives **8d** (Y = Cl), **8e** (Y = NO$_2$) and **9** was not possible due to the low solubility of these compounds in CDCl$_3$. However, the Δδ values of the isophthaloyl hosts **8d**, **8e** and **9** can be used to establish how similar these complexes are to the NMR solution structures that have been determined. There are some small differences in the Δδ values of the isophthaloyl host compounds containing the most electron-withdrawing groups. The largest differences are observed for the complexes of **8e** (Y = NO$_2$) with both the **15x** and **20x** series of bisaniline guests. The Δδ values of the *d* and *t* signals are lower than those seen in

the other complexes. The isophthaloyl derivative **8e** is likely to be a poorer H-bond acceptor and a better H-bond donor than the other isophthaloyl derivatives. A small population of the alternative mode of complexation shown in Fig. 11c is consistent with experimental Δδ values. The central isophthaloyl aromatic ring is moved out of the bisaniline pocket, accounting for the reduced Δδ values of *d* and *t*. Further support for the existence of this conformational equilibrium can be obtained from the Δδ values of the *s* signal, since this chemical shift is affected by the orientations of the adjacent amides (Fig. 13). Δδ Values of *s* are ~0.2 ppm larger in complexes with **8e** compared to the other

Table 5 Experimental (left) and calculated (right) ^{1}H NMR complexation-induced changes in chemical shift ($\Delta\delta$ in ppm) of the complexes in Fig. 12. The root mean squared deviations (RMSD) between experimental and calculated chemical shifts for each complex are indicated

Values given as experimental / calculated.

Complex	8a·15a	8a·15b	8a·15g	8a·20e	8a·20f	8b·15a	8b·20d	8b·20f	8c·20f
RMSD	0.05	0.16	0.14	0.11	0.12	0.14	0.16	0.09	0.13
Isophthaloyl host									
d	−0.34 / −0.33	−0.32 / −0.34	−0.48 / −0.47	−0.49 / −0.49	−0.57 / −0.59	−0.29 / −0.30	−0.44 / −0.45	−0.52 / −0.51	−0.53 / −0.53
t	−1.07 / −1.22	−1.08 / −1.10	−1.23 / −1.22	−1.48 / −1.47	−1.47 / −1.53	−0.97 / −1.02	−1.22 / −1.26	−1.34 / −1.35	−1.39 / −1.41
nh	1.46 / 1.43	1.55 / 1.56	1.34 / 1.31	1.66 / 1.65	1.62 / 1.63	1.58 / 1.56	1.78 / 1.78	1.74 / 1.74	1.76 / 1.74
aa	−0.14 / −0.13	−0.37 / −0.44	−0.06 / −0.02	−0.23 / −0.20	−0.14 / −0.12	−0.19 / −0.18	−0.19 / −0.18	−0.12 / −0.14	−0.14 / −0.17
me	−0.20 / −0.21	−0.38 / −0.39	−0.12 / −0.13	−0.24 / −0.26	−0.20 / −0.19	−0.25 / −0.20	−0.25 / −0.26	−0.22 / −0.21	−0.24 / −0.25
y	−0.02 / −0.02	−0.06 / −0.07	0.00 / −0.02	−0.02 / −0.05	0.03 / 0.04	so^b / so^b	−0.12 / −0.12	−0.04 / −0.02	0.01 / 0.02
Bisaniline guest									
p1	2.25 / 2.24	2.10 / 2.09	1.78 / 1.77	2.55 / 2.54	2.42 / 2.42	1.93 / 1.92	2.10 / 2.10	2.25 / 2.25	2.50 / 2.52
p2	−1.13 / −1.15	−1.00 / −1.08	−0.93 / −0.94	−0.84 / −0.85	−0.59 / −0.60	−1.10 / −1.05	−1.13 / −1.35	−1.17 / −1.16	−1.36 / −1.33
n1	2.07 / 2.16	1.94 / 1.85	1.70 / 1.73	2.70 / 2.70	2.52 / 2.48	1.97 / 1.98	2.24 / 2.24	2.71 / 2.71	1.89 / 1.91
m2	−0.12 / −0.08	−0.07 / −0.04	−0.10 / −0.10	0.07 / 0.08	0.04 / 0.04	−0.17 / −0.14	0.00 / 0.00	0.04 / 0.03	0.04 / 0.04
b1	0.02 / −0.01	0.03 / 0.06	0.03 / 0.02	−0.10 / −0.11	−0.09 / −0.09	0.00 / −0.01	−0.15 / −0.15	−0.11 / −0.11	−0.11 / −0.08
b2	0.12 / 0.15	0.13 / 0.11	0.13 / 0.18	0.07 / 0.07	0.08 / 0.08	0.14 / 0.12	0.02 / 0.01	0.08 / 0.08	0.08 / 0.06
b3	0.01 / 0.11	0.04 / 0.04	−0.02 / 0.02	0.16 / 0.17	0.17 / 0.15	0.01 / 0.01	0.21 / 0.16	0.18 / 0.18	0.15 / 0.16
b4	−0.20 / −0.20	−0.20 / −0.16	−0.20 / −0.21	0.07 / 0.09	0.06 / 0.06	−0.27 / −0.27	0.02 / 0.07	0.06 / 0.09	0.06 / 0.07
a1 m1	−0.20 / −0.21	−0.07 / −0.11	— / —	−0.21 / −0.19	−0.19 / —	−0.25 / −0.26	−0.34 / −0.36	— / —	— / —
a2	−0.11 / −0.11	−0.07 / −0.09	— / —	−0.36 / −0.38	−0.38 / —	−0.14 / −0.12	−0.14 / −0.13	— / —	— / —
a3	— / —	−0.12 / −0.14	— / —	— / —	— / —	— / —	— / —	— / —	— / —
a4	— / —	−0.15 / −0.18	— / —	— / —	— / —	— / —	— / —	— / —	— / —
a5	— / —	— / —	— / —	— / —	— / —	— / —	— / —	— / —	— / —

^{a} See Figs. 2 and 3 for proton labelling schemes. s and n2 are affected by polarisation, and by changes in the conformational distribution as discussed in the main text. They are excluded because neither of these effects are considered in the calculation of $\Delta\delta$ values. Titration experiments were repeated at least twice and $\Delta\delta$ is the weighted mean based on the observed % bound. ^{b} so—Not determined due to signal overlap.

isophthaloyl derivatives. If the +1.3 ppm $\Delta\delta$ value calculated for the b) to c) transition in Fig. 13 is accurate, then ~15% of the bound state of the complexes involving **8e** can be attributed to the binding mode shown in Fig. 13c. A second estimate of the position of the equilibrium can be obtained from the $\Delta\delta$ values of the **nh** protons in complexes involving **8e** compared with **8a**. Some of the shift of the **nh** protons in the well-behaved **8a** complexes will be caused by polarisation of the isophthaloyl amide when it accepts two H-bonds from the nitropyrrole unit of the bisaniline derivatives. The 10% increase in $\Delta\delta$ observed for the **nh** protons in complexes with **8e** *versus* **8a** is consistent with the 15% population of the alternative binding mode as estimated above (Fig. 11c and 13c).
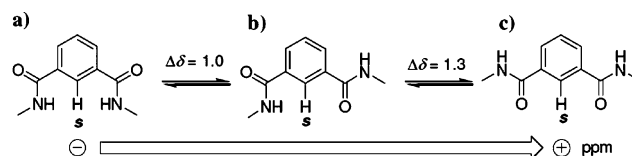

Fig. 13 The chemical shift of the **s** proton in isophthaloyl derivatives **8a**–**10** is influenced by the orientations of the amides. Chemical shift changes were calculated using HF/6-31G*.

The $\Delta\delta$ values of the **aa** and **me** signals on the terminal stacked aromatic rings in complexes with **8e** are similar to the other complexes, which suggests that the geometry of terminal stacking interaction in the conformational ensemble is not greatly affected by the alternative binding mode. The geometry of the stacking interaction in the alternative binding mode of **8e** is probably not identical to the main mode of complexation, because the bisaniline guest has to twist so that the amide carbonyl oxygens are the correct separation to accept two H-bonds from **8e**. The occurrence of the additional binding mode of **8e** is certainly not ideal, but $\Delta\delta$ values indicate that **8e** binds all bisaniline derivatives in a similar way, including the single-mutant compound **15g** (complex B in Fig. 1). Thus, the free energy differences arising from the alternative geometry of the minor mode of complexation are probably cancelled in the double-mutant cycle. The double-mutant cycle for complexes of **8e** measures the population-weighted average of the two similar (but probably not identical) stacking interactions shown in Fig. 11a and c.

Summary of conformational studies

In summary, ^{1}H NMR complexation-induced changes in chemical shift ($\Delta\delta$) have proved to be of exceptional utility for the characterisation of the supramolecular complexes used in this study. It has been possible to identify conformational complexities. Some complexes behaved as originally designed (complexes with **15a**, **15b**) and others behaved in unexpected ways that prevent valid double-mutant cycles from being constructed (complexes with **15c**, **15e** and **15f**). The information obtained from $\Delta\delta$ values has guided the design of compounds that overcame some of the conformational problems (**20d**, **20e** and **20f**). Small conformational differences in the complexes containing compound **8e** mean that some caution may need to be applied when interpreting the results where Y = NO$_2$.
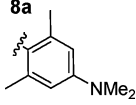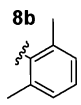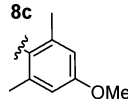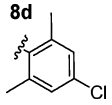
This journal is © The Royal Society of Chemistry 2007

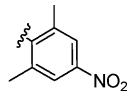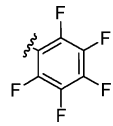*Org. Biomol. Chem.*, 2007, **5**, 1062–1080 | 1073
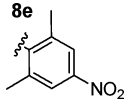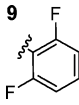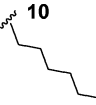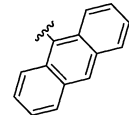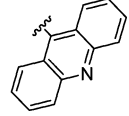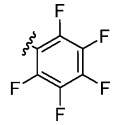
Double-mutant cycle results and discussion

The 1 : 1 association constants and free energies of complexation for all complexes used in this study are given in Table 6. Using the data in Table 6 and the equation from Fig. 1, the magnitude of the intermolecular stacking interaction was calculated for each of the aromatic pairs in Table 7. Although many of the values are the same within experimental error, the interactions range from +1.5 kJ mol^{-1} to −3.2 kJ mol^{-1} and are clearly sensitive to the nature of the aromatic substituents. Hammett substituent constants are frequently used in physical organic chemistry to rationalise electrostatic trends in experimental data.[68] In the work presented here, there is a mixture of *ortho* and *para* substituent

variations, in addition to the anthracene and pentafluorophenyl groups. This diverse cross-section of aromatic groups are not readily described using Hammett substituent constants. Instead, calculated electrostatic surface potentials (ESPs) have been used to generate a scale that describes the properties of the aromatic groups employed in this study.
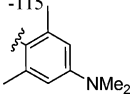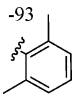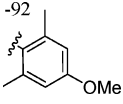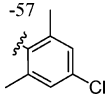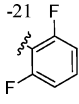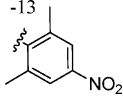
Fig. 14 shows the variation in the electrostatic potential surfaces of molecules representative of the aromatic groups used in binding studies. The values of the ESPs at the centre of the each aromatic group are included in Table 7. As has been noted by others, an OH or OMe substituent very slightly *reduces* the ESP at the ring centre, in accord with the small and positive Hammett *meta*-substituent constants (σ_m) of OH and OMe.[69,70] Since a subset

Table 6 Association constants (K_a in M^{-1}) and free energies of complexation (ΔG in kJ mol^{-1}) measured in CDCl$_3$ at 298 K[a]
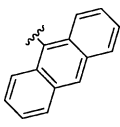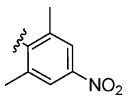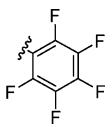
Bisaniline guest	Isophthaloyl host						
	8a (NMe$_2$)	8b	8c (OMe)	8d (Cl)	8e (NO$_2$)	9 (F)	10
15a	106 ± 18 −11.4 ± 0.4	69 ± 10 −10.3 ± 0.4	69 ± 11 −10.3 ± 0.4	70.1 ± 8 −10.4 ± 0.3	149 ± 31 −12.2 ± 0.5	56 ± 9 −9.8 ± 0.4	46 ± 3 −9.3 ± 0.1
15b	151 ± 30 −12.2 ± 0.5	70 ± 7 −10.3 ± 0.2	n.d.[b]	n.d.	175 ± 47 −12.6 ± 0.7	n.d.	54 ± 6
15c	116 ± 20 −11.6 ± 0.4	2 : 1[c]	n.d.	n.d.	128 ± 37 −11.8 ± 0.7	n.d.	2 : 1
15f	513 ± 113 −15.2 ± 0.5	133 ± 22 −11.9 ± 0.4	124 ± 29 −11.7 ± 0.6	n.d.	n.d.	n.d.	73 ± 16 −10.4 ± 0.5
15g	206 ± 44 −13.0 ± 0.5	83 ± 15 −10.8 ± 0.5	103 ± 20 −11.3 ± 0.5	69 ± 15 −10.3 ± 0.5	110 ± 28 −11.4 ± −0.6	66 ± 13 −10.2 ± 0.5	47 ± 5 −9.4 ± 0.3
20d	357 ± 82 −14.3 ± 0.8	248 ± 90 −13.4 ± 0.9	235 ± 69 −13.3 ± 0.7	234 ± 89 −13.3 ± 0.9	330 ± 223 −14.1 ± 1.7	111 ± 53 −11.5 ± 1.2	88 ± 23 −10.9 ± 0.6
20e	386 ± 94 −14.5 ± 0.6	196 ± 52 −12.9 ± 0.6	n.d.	n.d.	73 ± 22 −10.4 ± 0.7	n.d.	43 ± 4 −9.2 ± 0.2
20f	627 ± 206 −15.7 ± 0.8	227 ± 58 −13.2 ± 0.6	212 ± 53 −13.1 ± 0.6	94 ± 18 −11.1 ± 0.5	97 ± 26 −11.2 ± 0.7	68 ± 13 −10.3 ± 0.5	39 ± 7 −8.9 ± 0.4

[a] Titration experiments were repeated at least twice and K_a and ΔG are the weighted mean based on the observed chemical shift of the **d**, **t** and **nh** signals. Quoted errors are twice the standard error. [b] Not determined. [c] Binds as a 2 : 1 complex as described in the text.

Table 7 Aromatic stacking interaction energies ($\Delta\Delta G$ in kJ mol^{-1}) measured in CDCl$_3$ at 298 K. The electrostatic surface potentials (kJ mol^{-1}) of each group are indicated[a]

ESP	Aromatic group (on bisaniline guest)	Substituted aniline ring (on isophthaloyl host) ESP					
		−115 (NMe$_2$)	−93 (xylene)	−92 (OMe)	−57 (Cl)	−21 (F, F)	−13 (NO$_2$)
−92	(dimethylphenyl)	+1.5 ± 0.7	+0.4 ± 0.6	+0.9 ± 0.7	−0.1 ± 0.7	+0.3 ± 0.7	−0.8 ± 0.9
−54	(anthracenyl)	+1.1 ± 0.8	+0.8 ± 0.6	n.d.[b]	n.d.	n.d.	−0.8 ± 1.0
−21	(difluorophenyl)	+0.2 ± 1.2	−1.2 ± 1.2	−0.5 ± 1.1	−1.5 ± 1.3	+0.2 ± 1.6	−1.2 ± 1.9
−13	(dimethyl-nitrophenyl)	−1.7 ± 0.9	−2.3 ± 0.9	n.d.	n.d.	n.d.	+0.8 ± 1.0
+73	(pentafluorophenyl)	−3.2 ± 1.1	−2.9 ± 0.9	−2.2 ± 0.9	−1.2 ± 0.9	−0.5 ± 0.8	−0.2 ± 1.0

[a] Electrostatic surface potentials were calculated at the B3LYP/6-31G* level at the centre of each aromatic group. Titration experiments were repeated at least twice. Quoted errors are twice the standard error. [b] Not determined.

of the experimental stacking interaction energies reported here have previously been correlated against σ_m values,[55] it is valuable to know how σ_m relates to calculated ESPs. Very good agreement is observed between σ_m and the ESP at the ring centres of a series of *para*-substituted *meta*-xylenes (Fig. 15).[68] Similar plots using AM1 level calculations or σ_p were less good.

A plot of the experimental aromatic stacking interaction energies determined using the zipper complex double-mutant cycles against the ring centre ESPs of the aromatic groups in the isophthaloyl derivatives reveals some interesting general trends (Fig. 16). The stacking interaction of the negative surface of the dimethylphenyl group (red points in Fig. 16) with the most electron-rich aromatic group (Y = NMe$_2$) is the most repulsive interaction encountered in these studies. As the ESP of the partner ring becomes less negative, the stacking interaction becomes less repulsive. The pentafluorophenyl group (blue points) has a positive surface and it interacts most favourably with electron-rich aromatics, inverting the interaction trend seen for the dimethylphenyl group. The groups of Gung and Siegel observed similar effects in intramolecular systems.[32,71] For all of the interaction trends, as the ESP on the interacting partner approaches zero, then so does the magnitude of stacking interaction. The ESPs of the

difluorophenyl (yellow points) and nitrophenyl (green points) groups are part way between those of the pentafluorophenyl (blue points) and dimethylphenyl groups (red points), and accordingly, their stacking interaction energies are generally found to lie between those of the pentafluorophenyl and dimethylphenyl groups.

While the major trends in the aromatic stacking interaction energies can be attributed to electrostatic effects using the very simplistic model described above, this is not the complete picture. For example, why are there favourable stacking interactions between the nitro-substituted aromatic groups and electron-rich aromatics, when the ESPs of the nitro-substituted rings also have partial negative charges? This discrepancy arises because the ring-centre ESP model is too simple to fully describe the interactions that have been measured. Clearly, when two aromatic rings stack upon one another the surfaces of the rings are brought into contact and so are the substituents. In an offset-stacked conformation, the ring substituents may also come into contact with the surface of the aromatic ring.[21,30,72] The NMR solution structures in Fig. 12 indicate that the *ortho*-methyl (or fluorine) substituents are positioned close to the *ortho* carbon of the opposing ring. The methyl groups in *o*-dimethyl-*p*-nitrophenyl (Fig. 14h) are rather
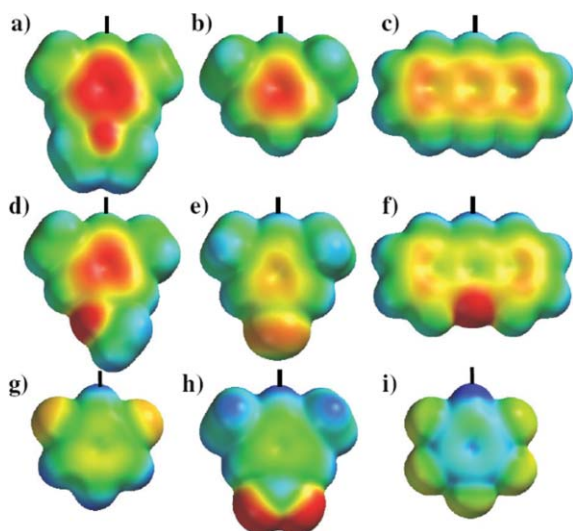
This journal is © The Royal Society of Chemistry 2007

Org. Biomol. Chem., 2007, **5**, 1062–1080 | 1075

Fig. 14 B3LYP/6-31G* calculated electrostatic potential surfaces (ESPs) of molecules representative of the stacking aromatic groups used in this study. Position 1 in the compound nomenclature used refers to the position at which the group is connected to the isophthaloyl or bisaniline derivative in the zipper complex; a) 2,6-dimethyl-4-dimethylaminobenzene, b) 2,6-dimethylbenzene, c) anthracene, d) 2,6-dimethyl-4-methoxybenzene, e) 4-chloro-2,6-dimethylbenzene, f) acridine, g) 2,6-difluorobenzene, h) 2,6-dimethyl-4-nitrobenzene, i) pentafluorobenzene. Colours are scaled from −100 to +100 kJ mol^{-1} (red to blue), green represents neutral charge.

polar, with an ESP of +79 kJ mol^{-1}, a value similar to the ring centre of a pentafluorophenyl group. This explains the favourable interaction between the nitro-substituted aromatics and electron-rich rings.

All of the aromatic groups used in this study contain *ortho*-methyl or fluorine substituents, and our data contain further evidence of the importance of substituent-to-ring interactions in the zipper complexes. As mentioned earlier, there is a clear trend for the dimethylphenyl stacking interactions (red line in Fig. 16). The sole significant departure from this trend corresponds to the stacking interaction with the difluoroaniline group (ring centre
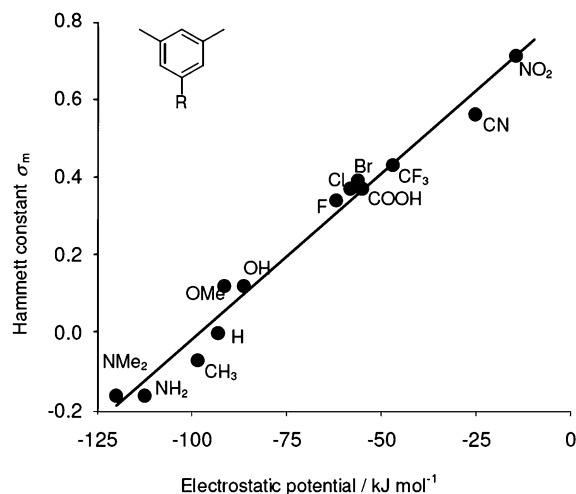

Fig. 15 B3LYP/6-31G* electrostatic surface potentials (ESPs) at the ring centres of *para*-substituted *meta*-xylenes correlate well with Hammett *meta*-substituent constants that have been previously used in structure activity relationships describing aromatic stacking interactions.

ESP −21 kJ mol^{-1}). Although the ESP at the ring centre of the difluorophenyl ring is similar to that of the nitro-substituted ring, the polar methyl groups (+79 kJ mol^{-1}) have been replaced by fluorine substituents with a partial negative charge (−42 kJ mol^{-1}). Thus, the favourable polar CH$_3$–π interaction is replaced by a small but repulsive F–π interaction. Using this departure from the dimethylphenyl trend line, an upper limit for the CH$_3$–π interaction in this complex can be tentatively assigned as −1.0 kJ mol^{-1}. Interestingly, this value is similar to the intercept of the red line in Fig. 16. In other words, the contribution from the stacking interaction is approximately zero when the ESP at the centre of the aniline ring is zero, but there is an additional contribution from attractive CH$_3$–π interactions.

The stacking interactions of the pentafluorophenyl group (blue points in Fig. 16) appear to be better described using a simple ring-centre ESP model, and this trend line meets the y-axis close to the origin. This may be explained by the relative simplicity of the ESP
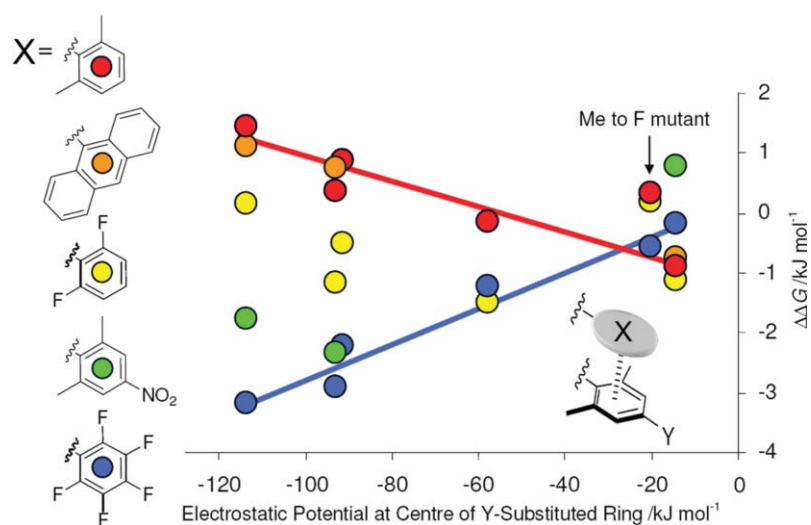

Fig. 16 Plot of experimental aromatic stacking interaction energies measured in zipper complexes (y-axis) against the B3LYP/6-31G* calculated electrostatic surface potential at the ring centre of substituted isophthaloyl derivatives (Y = NMe$_2$ to Y = NO$_2$) (x-axis).

distribution over the surface of the pentafluorophenyl group. The centre of the pentafluorophenyl group has partial positive charge, but the ESPs of the fluorine substituents at the face of the ring are close to zero (*cf.* the partial negative charge of the fluorine substituents in the difluorophenyl group). This means that the trend in the interaction energies for the pentafluorophenyl group is not complicated by electrostatic interactions involving the fluorine substituents.

The *o*-dimethylphenyl·difluorophenyl and the *o*-dimethylphenyl·*o*-dimethyl-*p*-nitrophenyl stacking interactions have been measured twice; once with the dimethylphenyl group present in the isophthaloyl host (**8b·20d**) and again with the dimethylphenyl group in the bisaniline guest (**9·15a**). While the stacking interactions that are reported are the same within the quoted error margins, it may be more than a coincidence that in both cases, the interaction is 1.5 kJ mol⁻¹ more stable when the dimethylphenyl ring is contained within the isophthaloyl host. It is important to note that the geometry of the stacking interaction in the zipper complexes is not symmetrical, and that the relative orientation of the rings depends on which half of the complex the aromatic group is attached to. The difference in the interaction energies may be an indication of how sensitive aromatic stacking interactions are to subtle changes in geometry and suggests that the geometric constraints of the zipper architecture prevents the aromatic groups from reaching the minimum energy arrangement. However, without the ability to fix the geometry of the interaction, it would not have been possible to examine the effects of substituents which would otherwise be obscured by structural differences.

Theoretical calculations of aromatic interactions in the gas phase have indicated that electrostatic interactions provide less of a contribution to the total interaction energy than van der Waals interactions (consisting of dispersion, induction and repulsion terms).[16,18–21,59,73–75]

The experimental studies of Wilcox and co-workers, and Nakamura and Houk, have suggested that dispersion forces make important contributions in edge-to-face aromatic interactions.[76–78] However, recent insights have shown that solvent competition provides a more general explanation for the behaviour of the torsion balance molecules employed in these studies.[79,80]

From a simple consideration of relative areas of molecular contact, dispersion interactions should be expected to contribute more to aromatic stacking energies compared with aromatic edge-to-face interactions. Gas phase calculations predict that stacking free energies of all substituted benzene dimers are more stable than the unsubstituted stacked benzene dimer. Thus, electron-donating substituents have been predicted to stabilise aromatic stacking interactions even when both π-faces are electron-rich.

Mei and Wolf found that the degree of splay between two acridine groups forced into an intramolecular stack decreased upon sequential oxidation to the mono-*N*-oxide and the di-*N*,*N'*-oxide.[37] The change in geometry was attributed to an increase in the stability of the stacking interaction between the acridine rings. This observation was cited as experimental support for the computational predictions of Sherrill and co-workers, since the authors believed that *N*-oxidation *increased* the electron density of acridine.[21] On the contrary, the nitrogen atom in acridine *N*-oxide bears a formal positive charge and the electron density of the entire acridine π-face is decreased, a fact supported by DFT/6-31G*

electrostatic surface potentials (not shown). Although dispersion interactions are almost certainly important to the overall stability of these compounds, the conformational changes and inferred changes in the stacking interactions are in perfect accord with the results of Siegel, Gung and those presented in the current study.[28,31,32,55] *i.e.* the negative charge on the π-face of acridine is reduced by *N*-oxidation, which decreases electrostatic repulsion between the rings. Additionally, the skewed arrangement of the rings in the acridyl di-*N*,*N'*-oxide can be attributed to electrostatic repulsion between the negatively charged oxygen atoms.

The strained intramolecular systems employed by Siegel and Wolf for the investigation of aromatic stacking interactions represent a special case where the solvent is completely excluded from interaction of interest.[28,29,37] The intermolecular approach taken in the current study is able to provide additional insights into the contribution of van der Waals interactions to aromatic stacking interactions in the solution phase. At this point it is important to note that although the binding experiments were performed in CDCl₃, much of the solvent may be displaced from the terminal aromatic rings by the mutant alkyl groups in the reference complexes in the double-mutant cycle (Fig. 1). This means that the measured aromatic interaction energies effectively refer to an alkane pseudo-solvent environment rather than CDCl₃.

Anthracene has a higher polarisability than simple aromatics,[81] yet the stacking interactions of the anthracene group (orange points in Fig. 16) are practically identical to those obtained with the smaller dimethylphenyl group (red points) and follow the same electrostatic trend as the aniline ring Y-substituent is varied. Any contributions from differences in dispersion interactions in the anthracene stacking interactions are small enough to be masked by electrostatic effects and the experimental errors. Dispersion interactions play a lesser role in solution compared to the gas phase because of competitive dispersion interactions with the solvent. When a stacking interaction forms between two aromatic rings, the solvent molecules coating the interacting surfaces are displaced. Thus, if the solvent is able to coat the entire surface of the rings evenly, the favourable free energy of the dispersion interaction between the stacked aromatic rings will be reduced by the cost of breaking the dispersion interactions of each aromatic group with the solvent. Theory suggests that there is little variation of the dispersion interaction energy per unit surface area for intermolecular interactions between organic molecules, and so we should expect electrostatic effects to dominate in solution.[80,82]

Experimental

Computational procedures

Ab initio calculations were performed using Spartan, Wavefunction, Inc., Irvine, CA, USA. Molecular modelling was performed using XED 6.1.0, Cresset BioMolecular Discovery Ltd., Hertfordshire, UK.

General NMR procedures

¹H, ¹⁹F and ¹³C spectra were recorded on either a Bruker AC250 or a AMX400 spectrometer with residual solvent as an internal standard. Fluorine chemical shifts were referenced to an external CFCl₃ reference. Two-dimensional ROESY experiments were

This journal is © The Royal Society of Chemistry 2007

Org. Biomol. Chem., 2007, **5**, 1062–1080 | 1077

recorded on a Bruker AMX400 with 300 ms mixing time and a 3 s relaxation delay between pulses.

¹H NMR dilutions

A saturated analyte solution of known concentration (~mM) was prepared in CDCl₃. Aliquots of this solution were sequentially added to a small volume (0.25–0.5 ml) of CDCl₃ in an NMR tube, and the ¹H NMR chemical shifts for each signal were recorded. The program NMRDil_Dimer was used to fit data to a dimerisation isotherm using a non-linear curve fitting procedure. Dimerisation constants and the chemical shifts of the dimer and free analyte were determined for each signal monitored. Dilution experiments were performed in duplicate and the weighted mean dimerisation constant (based on the observed changes in chemical shift) was used in the fitting of NMR titration data as outlined below.

¹H NMR titrations

A few ml of host solution of known concentration (0.2–5 mM) was prepared in CDCl₃. A small sample (0.2–0.5 ml) of this solution was added to an NMR tube, and a ¹H NMR spectrum was recorded. A guest solution of known concentration (7–40 mM) was then prepared using the remaining host solution. This solution was saturated with guest to allow as much coverage of the binding isotherm as possible (generally 50%–90% was achieved). This procedure also ensured that the concentration of host remained constant throughout the titration. Aliquots of the saturated guest solution were added successively to the NMR tube containing the host solution, and the ¹H NMR spectrum was recorded after each addition. The program NMRTit_HGHHGG was used to fit host signals to a 1 : 1 binding isotherm allowing for dimerisation of the guest using a non-linear curve fitting procedure. For titrations with compounds **20d** and **20f** the concentration of guest was corrected to allow for the presence of ~30% inactive conformer as determined by relative integrals of the *me* and *me+* ¹H NMR signals. The mean association constant for each experiment was evaluated as the weighted mean based on the observed change in chemical shift for the *d*, *t* and *nh* signals in all complexes (for proton labelling scheme see Fig. 2 and 3). The error was taken as twice the standard error.

Limiting complexation-induced chemical shifts of the **15x** and **20x** guest signals (Table 4) were extrapolated by determining the relative concentrations of complex [HG], free guest [G], guest dimer [GG], and the values of the guest chemical shifts in these three states. Since the concentration of host was constant throughout the titration (and low enough that dimerisation was insignificant), the host concentration was in excess of the guest during the early stages of a titration. Under these conditions, complexation provides a larger contribution to the observed chemical shifts of the guest than guest dimerisation. The concentration of complex (and therefore complexed guest) is given by:

$$[HG] = [H]_0 \left(\Delta\delta_{obsH} / \Delta\delta_{boundH} \right) \quad (1)$$

where $[H]_0$ is the total concentration of host, the observed change in chemical shift of a particular host signal is $\Delta\delta_{obsH}$, and $\Delta\delta_{boundH}$ is the limiting complexation-induced change in chemical shift of the host as determined from the NMR titration experiment. The

free concentration of guest in this system can be shown to be:

$$[G] = \frac{-1 + \sqrt{1 + 8K_{dimG}([G]_0 - [HG])}}{4K_{dimG}} \quad (2)$$

and the concentration of guest dimer is:

$$[GG] = K_{dimG}[G]^2 \quad (3)$$

where K_{dimG} is the dimerisation constant of G determined from NMR dilution experiments. The observed chemical shift of the guest signal has three contributing terms:

$$\delta_{obsG} = \frac{[HG]}{[G]_0}\delta_{boundG} + \frac{[G]}{[G]_0}\delta_{freeG} + 2\frac{[GG]}{[G]_0}\delta_{dimG} \quad (4)$$

where $[G]_0$ is the total concentration of guest, δ_{boundG}, δ_{freeG} and δ_{dimG} are the chemical shifts of a guest signal in the three states [HG], [G] and [GG] respectively. The concentrations in this equation are known from eqn (1)–(3), and δ_{freeG} and δ_{dimG} were determined in the NMR dilution experiment. Thus, the equation can be rearranged to yield the desired limiting complexation-induced chemical shift of a particular guest signal, δ_{boundG}. The difference between this number and δ_{freeG} gives the limiting complexation-induced change in chemical shift which is referred to as the guest $\Delta\delta$ elsewhere in this report.

NMR structure determination

The method used to determine three-dimensional structures from limiting changes in complexation-induced chemical shift $\Delta\delta$ has been described in detail elsewhere.[65] Molecules were built and minimised using standard bond lengths and angles in XED.[62] Ring current factors used in the calculation of $\Delta\delta$ values, relative to the phenyl group, were: pyrrole 0.55, central anthracene ring 1.27, outer anthracene rings 0.8. Ring currents for the anthracene group were based on ring currents calculated by Fowler and Steiner.[83] A genetic algorithm was used to optimise the conformation of the complex so that the calculated $\Delta\delta$ values matched the experimental values as closely as possible (Table 5). The structure of each complex was refined using a population of 2000, a replacement rate of 400 per generation and five sequential steps of 1000 generations. The first step allowed intermolecular translations of ±10 Å, rotations of ±360° and intramolecular torsional changes of ±360° for the bonds highlighted in Fig. 17. After each step, the calculated structure in closest agreement with experimental $\Delta\delta$ values was used to generate a new population of 2000, and the search space was reduced by a half in all
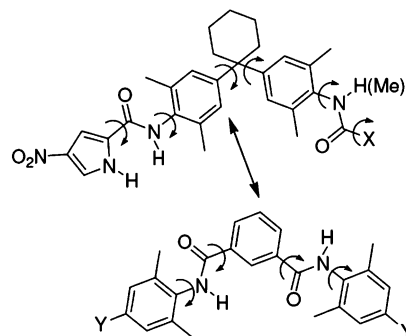

Fig. 17 The bond torsions that were free to rotate during the NMR solution structure determination and the intermolecular NOE constraint are indicated. X groups are shown in Fig. 3.

dimensions: intermolecular translations (±5 Å, 2.5 Å, 1.25 Å), rotations (±180°, 90°, 45°, 22.5°) and torsions (±180°, 90°, 45°, 22.5°). The solubilising R group and piperidine protons did not move in NMR experiments and were therefore excluded from calculations. van der Waals clashes were penalised at distances of less than 2 Å for intermolecular clashes and 1 Å for intramolecular clashes for non-hydrogen atoms. The NOE constraint illustrated in Fig. 17 was imposed by applying a penalty, if the inter-proton separation exceeded 5 Å. Each geometry optimisation was run at least five times. Structure calculations yielding RMSDs between calculated and experimental $\Delta\delta$ values less than 0.17 ppm were accepted. The optimised structures obtained from repeat calculations of the complexes shown in Fig. 12 were very similar, but only the structures with the lowest RMSDs are reported in this work.

Synthetic procedures

Detailed synthetic procedures and compound characterisation data are provided in the ESI.†

Conclusions

Aromatic stacking interactions are sensitive to changes in geometry and the degree of overlap. Using H-bonded supramolecular zipper complexes, it has been possible to lock the geometry of two aromatic rings in an offset stacked arrangement. This has enabled the effects of substituents on the interaction free energy to be quantified. The conformational behaviour of the complexes in the solid state and in solution has been thoroughly investigated. Some complexes were found to be incompatible with the double-mutant cycle methodology and were excluded from the analysis due to significant conformational changes. Insights obtained from these conformational studies guided the design and synthesis of new compounds better suited to the approach. To a first approximation, the electrostatic properties of the ring surfaces dominate the trends in the interaction energy. However, direct electrostatic interactions with the ring substituents also make important contributions. The interplay of these two factors could lead to complicated behaviour, for example, quite different interactions between similar aromatic groups in different contexts.

References

1 B. R. Hamilton and D. L. Hammick, *J. Chem. Soc.*, 1938, 1350–1352.
2 D. B. Amabilino and J. F. Stoddart, *Chem. Rev.*, 1995, **95**, 2725–2829.
3 H. C. Kolb, P. G. Andersson and K. B. Sharpless, *J. Am. Chem. Soc.*, 1994, **116**, 1278–1291.
4 M. Keller, C. Lehmann and M. Mutter, *Tetrahedron*, 1999, **55**, 413–422.
5 B. M. Trost, D. O'Krongly and J. L. Belleitre, *J. Am. Chem. Soc.*, 1980, **102**, 7595–7596.
6 M. Weck, A. R. Dunn, K. Matsumoto, G. W. Coates, E. B. Lobkovsky and R. H. Grubbs, *Angew. Chem., Int. Ed.*, 1999, **38**, 2741–2745.
7 G. J. Gabriel, S. Sorey and B. L. Iverson, *J. Am. Chem. Soc.*, 2005, **127**, 2637–2640.
8 G. J. Gabriel and B. L. Iverson, *J. Am. Chem. Soc.*, 2002, **124**, 15174–15175.
9 K. M. Guckian, B. A. Schweitzer, R. X. F. Ren, C. J. Sheils, D. C. Tahmassebi and E. T. Kool, *J. Am. Chem. Soc.*, 2000, **122**, 2213–2222.
10 W. Saenger, *Principles of Nucleic Acid Structure*, Spring-Verlag, New York, 1988.
11 G. B. McGaughey, M. Gagne and A. K. Rappe, *J. Biol. Chem.*, 1998, **273**, 15458–15463.
12 P. A. Williams, J. Cosme, A. Ward, H. C. Angove, D. M. Vinkovic and H. Jhoti, *Nature*, 2003, **424**, 464–468.
13 G. Kryger, I. Silman and J. L. Sussman, *Structure (London)*, 1999, **7**, 297–307.
14 G. Kryger, I. Silman and J. L. Sussman, *J. Physiol. (Paris)*, 1998, **92**, 191–194.
15 D. F. V. Lewis, M. N. Jacobs and M. Dickins, *Drug Discovery Today*, 2004, **9**, 530–537.
16 S. Tsuzuki, K. Honda, T. Uchimaru, M. Mikami and K. Tanabe, *J. Am. Chem. Soc.*, 2002, **124**, 104–112.
17 S. Perez-Casas, J. Hernandez-Trujillo and M. Costas, *J. Phys. Chem. B*, 2003, **107**, 4167–4174.
18 M. O. Sinnokrot and C. D. Sherrill, *J. Am. Chem. Soc.*, 2004, **126**, 7690–7697.
19 M. O. Sinnokrot and C. D. Sherrill, *J. Phys. Chem. A*, 2003, **107**, 8377–8379.
20 M. O. Sinnokrot and C. D. Sherrill, *J. Phys. Chem. A*, 2004, **108**, 10200–10207.
21 A. L. Ringer, M. O. Sinnokrot, R. P. Lively and C. D. Sherrill, *Chem.–Eur. J.*, 2006, **12**, 3821–3828.
22 B. W. Gung and J. C. Amicangelo, *J. Org. Chem.*, 2006, **71**, 9261–9270.
23 C. A. Hunter and J. K. M. Sanders, *J. Am. Chem. Soc.*, 1990, **112**, 5525–5534.
24 C. A. Hunter, K. R. Lawson, J. Perkins and C. J. Urch, *J. Chem. Soc., Perkin Trans. 2*, 2001, 651–669.
25 M. L. Waters, *Curr. Opin. Chem. Biol.*, 2002, **6**, 736–741.
26 E. A. Meyer, R. K. Castellano and F. Diederich, *Angew. Chem., Int. Ed.*, 2003, **42**, 1210–1250.
27 M. L. Waters, *Biopolymers*, 2004, **76**, 435–445.
28 F. Cozzi and J. S. Siegel, *Pure Appl. Chem.*, 1995, **67**, 683–689.
29 F. Cozzi, R. Annunziata, M. Benaglia, M. Cinquini, L. Raimondi, K. K. Baldridge and J. S. Siegel, *Org. Biomol. Chem.*, 2003, **1**, 157–162.
30 M. J. Rashkin and M. L. Waters, *J. Am. Chem. Soc.*, 2002, **124**, 1860–1861.
31 B. W. Gung, X. Xue and H. J. Reich, *J. Org. Chem.*, 2005, **70**, 3641–3644.
32 B. W. Gung, M. Patel and X. Xue, *J. Org. Chem.*, 2005, **70**, 10532–10537.
33 M. S. Cubberley and B. L. Iverson, *J. Am. Chem. Soc.*, 2001, **123**, 7560–7563.
34 L. F. Newcomb and S. H. Gellman, *J. Am. Chem. Soc.*, 1994, **116**, 4993–4994.
35 R. R. Gardner, S. L. McKay and S. H. Gellman, *Org. Lett.*, 2000, **2**, 2335–2338.
36 S. L. McKay, B. Haptonstall and S. H. Gellman, *J. Am. Chem. Soc.*, 2001, **123**, 1244–1245.
37 X. Mei and C. Wolf, *J. Org. Chem.*, 2005, **70**, 2299–2305.
38 M. Gray, A. J. Goodman, J. B. Carroll, K. Bardon, M. Markey, G. Cooke and V. M. Rotello, *Org. Lett.*, 2004, **6**, 385–388.
39 R. Faraoni, M. Blanzat, S. Kubicek, C. Braun, W. B. Schweizer, V. Gramlich and F. Diederich, *Org. Biomol. Chem.*, 2004, **2**, 1962–1964.
40 T. Yajima, R. Takamido, Y. Shimazaki, A. Odani, Y. Nakabayashi and O. Yamauchi, *Dalton Trans.*, 2007, 299–307.
41 S. L. Cockroft and C. A. Hunter, *Chem. Soc. Rev.*, 2007, DOI: 10.1039/b603842p.
42 S. M. Butterfield and J. Rebek, *J. Am. Chem. Soc.*, 2006, **128**, 15366–15367.
43 H. Adams, F. J. Carver, C. A. Hunter, J. C. Morales and E. M. Seward, *Angew. Chem., Int. Ed. Engl.*, 1996, **35**, 1542–1544.
44 H. Adams, K. D. M. Harris, G. A. Hembury, C. A. Hunter, D. Livingstone and J. F. McCabe, *Chem. Commun.*, 1996, 2531–2532.
45 F. J. Carver, C. A. Hunter and E. M. Seward, *Chem. Commun.*, 1998, 775–776.
46 H. Adams, P. L. Bernad, Jr., G. A. Hembury, C. A. Hunter, J. F. McCabe, D. S. Eggleston, R. C. Haltiwanger, D. J. Livingstone, K. D. M. Harris and B. M. Kariuki, *Chem. Commun.*, 2001, 1500–1501.
47 H. Adams, J.-L. J. Blanco, G. Chessari, C. A. Hunter, C. M. R. Low, J. M. Sanderson and J. G. Vinter, *Chem.–Eur. J.*, 2001, **7**, 3494–3503.
48 F. J. Carver, C. A. Hunter, P. S. Jones, D. J. Livingstone, J. F. McCabe, E. M. Seward, P. Tiger and S. E. Spey, *Chem.–Eur. J.*, 2001, **7**, 4854–4862.
49 F. J. Carver, C. A. Hunter, D. J. Livingstone, J. F. McCabe and E. M. Seward, *Chem.–Eur. J.*, 2002, **8**, 2847–2859.
50 C. A. Hunter, C. M. R. Low, C. Rotger, J. G. Vinter and C. Zonta, *Proc. Natl. Acad. Sci. U. S. A.*, 2002, **99**, 4873–4876.
51 C. A. Hunter, C. M. R. Low, C. Rotger, J. G. Vinter and C. Zonta, *Chem. Commun.*, 2003, 834–835.

This journal is © The Royal Society of Chemistry 2007

Org. Biomol. Chem., 2007, **5**, 1062–1080 | 1079

52 C. A. Hunter, C. M. R. Low, J. G. Vinter and C. Zonta, *J. Am. Chem. Soc.*, 2003, **125**, 9936–9937.
53 H. Adams, S. L. Cockroft, C. Guardigli, C. A. Hunter, K. R. Lawson, J. Perkins, S. E. Spey, C. J. Urch and R. Ford, *ChemBioChem*, 2004, **5**, 657–665.
54 H. Adams, C. A. Hunter, K. R. Lawson, J. Perkins, S. E. Spey, C. J. Urch and J. M. Sanderson, *Chem.–Eur. J.*, 2001, **7**, 4863–4877.
55 S. L. Cockroft, C. A. Hunter, K. R. Lawson, J. Perkins and C. J. Urch, *J. Am. Chem. Soc.*, 2005, **127**, 8594–8595.
56 I. Azumaya, K. Yamaguchi, H. Kagechika, S. Saito, A. Itai and K. Shudo, *Yakugaku Zasshi*, 1994, **114**, 414–430.
57 A. Spitaleri, C. A. Hunter, J. F. McCabe, M. J. Packer and S. L. Cockroft, *CrystEngComm*, 2004, **6**, 489–493.
58 C. R. Patrick and G. S. Prosser, *Nature*, 1960, 1021.
59 P. Mignon, S. Loverix, J. Steyaert and P. Geerlings, *Nucleic Acids Res.*, 2005, **33**, 1779–1789.
60 F. Ponzini, R. Zagha, K. Hardcastle and J. S. Siegel, *Angew. Chem., Int. Ed.*, 2000, **39**, 2323–2325.
61 J. C. Collings, K. P. Roscoe, E. G. Robins, A. S. Batsanov, L. M. Stimson, J. A. K. Howard, S. J. Clark and T. B. Marder, *New J. Chem.*, 2002, **26**, 1740–1746.
62 J. G. Vinter, *J. Comput.-Aided Mol. Des.*, 1994, **8**, 653–668.
63 A. Itai, Y. Toriumi, N. Tomioka, H. Kagechika, I. Azumaya and K. Shudo, *Tetrahedron Lett.*, 1989, **30**, 6177–6180.
64 C. A. Hunter, M. J. Packer and C. Zonta, *Prog. Nucl. Magn. Reson. Spectrosc.*, 2005, **47**, 27–39.
65 C. A. Hunter and M. J. Packer, *Chem.–Eur. J.*, 1999, **5**, 1891–1897.
66 M. Gardner, A. J. Guerin, C. A. Hunter, U. Michelsen and C. Rotger, *New J. Chem.*, 1999, **23**, 309–316.
67 C. A. Hunter, C. M. R. Low, M. J. Packer, S. E. Spey, J. G. Vinter, M. O. Vysotsky and C. Zonta, *Angew. Chem., Int. Ed.*, 2001, **40**, 2678–2682.
68 C. Hansch, A. Leo and R. W. Taft, *Chem. Rev.*, 1991, **91**, 165–195.
69 S. Mecozzi, A. P. West, Jr. and D. A. Dougherty, *Proc. Natl. Acad. Sci. U. S. A.*, 1996, **93**, 10566–10571.
70 F. Hof, D. M. Scofield, W. B. Schweizer and F. Diederich, *Angew. Chem., Int. Ed.*, 2004, **43**, 5056–5059.
71 F. Cozzi, F. Ponzini, R. Annunziata, M. Cinquini and J. S. Siegel, *Angew. Chem., Int. Ed. Engl.*, 1995, **34**, 1019–1020.
72 B. W. Gung, X. Xue and H. J. Reich, *J. Org. Chem.*, 2005, **70**, 7232–7237.
73 E. C. Lee, B. H. Hong, J. Y. Lee, J. C. Kim, D. Kim, Y. Kim, P. Tarakeshwar and K. S. Kim, *J. Am. Chem. Soc.*, 2005, **127**, 4530–4537.
74 P. Mignon, S. Loverix and P. Geerlings, *Chem. Phys. Lett.*, 2005, **401**, 40–46.
75 A. Olasz, P. Mignon, F. De Proft, T. Veszpremi and P. Geerlings, *Chem. Phys. Lett.*, 2005, **407**, 504–509.
76 S. Paliwal, S. Geib and C. S. Wilcox, *J. Am. Chem. Soc.*, 1994, **116**, 4497–4498.
77 E.-i. Kim, S. Paliwal and C. S. Wilcox, *J. Am. Chem. Soc.*, 1998, **120**, 11192–11193.
78 K. Nakamura and K. N. Houk, *Org. Lett.*, 1999, **1**, 2049–2051.
79 T. Ren, Y. Jin, K. S. Kim and D. H. Kim, *J. Biomol. Struct. Dyn.*, 1997, **15**, 401–405.
80 S. L. Cockroft and C. A. Hunter, *Chem. Commun.*, 2006, 3806–3808.
81 D. R. E. Lide, *CRC Handbook of chemistry and physics*, 75th edn, CRC Press, Boca Raton, 1994.
82 C. A. Hunter, *Angew. Chem., Int. Ed.*, 2004, **43**, 5310–5324.
83 P. W. Fowler and E. Steiner, *Chem. Phys. Lett.*, 2002, **364**, 259–266.

1080 | *Org. Biomol. Chem.*, 2007, **5**, 1062–1080

This journal is © The Royal Society of Chemistry 2007